iScience

CellPress
OPEN ACCESS

Article

Requirement of PP2A-B56^{Par1} for the Stabilization of the CDK Inhibitor Rum1 and Activation of APC/C^{Ste9} during Pre-Start G1 in *S. pombe*

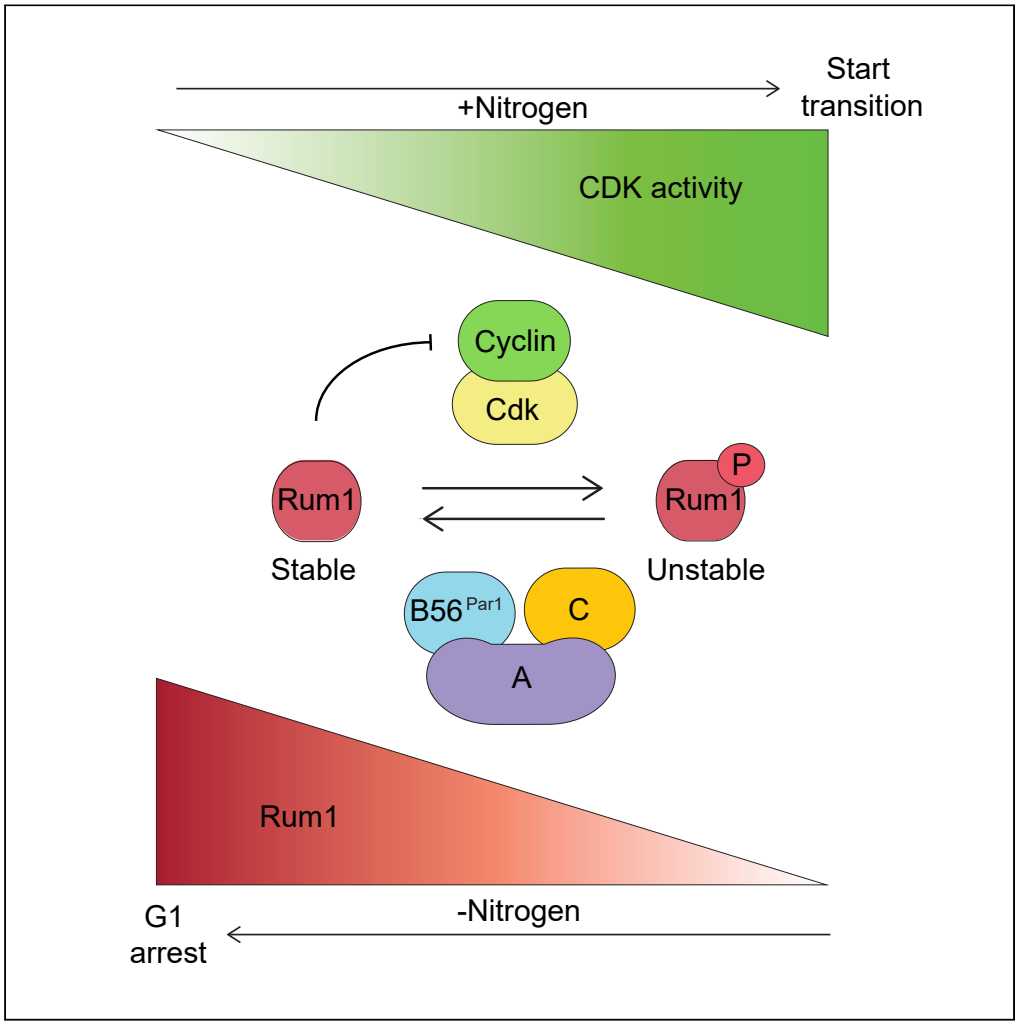

Vilte Stonyte, Ruth Martín, Dario Segura-Peña, Nikolina Sekulić, Sandra Lopez-Aviles

r.m.martin@ncmm.uio.no (R.M.)
sandra.lopez-aviles@ncmm.uio.no (S.L.-A.)

HIGHLIGHTS

PP2A-B56^{Par1} is required for cell-cycle arrest and mating upon nitrogen deprivation

Loss of Par1 impairs degradation of Cdc13 under nitrogen starvation

Absence of Par1 impedes proper dephosphorylation of Ste9 and accumulation of Rum1

Mutation of a Rum1 putative PP2A-B56 SLiM depicts similar defects as the loss Par1

Stonyte et al., iScience *23*, 101063
May 22, 2020
https://doi.org/10.1016/j.isci.2020.101063

iScience

CellPress
OPEN ACCESS

Article

Requirement of PP2A-B56^{Par1} for the Stabilization of the CDK Inhibitor Rum1 and Activation of APC/C^{Ste9} during Pre-Start G1 in *S. pombe*

Vilte Stonyte,[1,4] Ruth Martín,[1,4,*] Dario Segura-Peña,[1] Nikolina Sekulić,[1,2] and Sandra Lopez-Aviles[1,3,4,5,*]

SUMMARY

Exit from the cell cycle during the establishment of quiescence and upon cell differentiation requires the sustained inactivation of CDK complexes. Fission yeast cells deprived of nitrogen halt cell cycle progression in pre-Start G1, before becoming quiescent or undergoing sexual differentiation. The CDK inhibitor Rum1 and the APC/C activator Ste9 are fundamental for this arrest, but both are down-regulated by CDK complexes. Here, we show that PP2A-B56^{Par1} is instrumental for Rum1 stabilization and Ste9 activation. In the absence of PP2A-B56^{Par1}, cells fail to accumulate Rum1, and this results in persistent CDK activity, Ste9 inactivation, retention of the mitotic cyclin Cdc13, and impaired withdrawal from the cell cycle during nitrogen starvation. Importantly, mutation of a putative B56 interacting motif in Rum1 recapitulates these defects. These results underscore the relevance of CDK-counteracting phosphatases in cell differentiation, establishment of the quiescent state, and escape from it in cancer cells.

INTRODUCTION

In all organisms, from the simplest prokaryote up to humans, cells have the ability to withdraw from the cell cycle when their environment does not support cell proliferation. In metazoans, a majority of the cells lie in a quiescent, non-dividing state prompted by signals emanating from the microenvironment and by the geometrical constraints that occur within tissues (reviewed in Fiore et al., 2018). However, they can re-enter the mitotic cycle upon stimulation when new cells are needed to replace old ones, or in the case of injury (reviewed in O'Farrell, 2011). Thus, maintaining the right balance between quiescence and proliferation is essential for tissue homeostasis and repair. Conversely, loss of this balance can lead to hyperproliferative diseases such as cancer. Cell-cycle exit is also intimately linked to the process of cell differentiation. As cells become more differentiated, their ability to proliferate decreases, to the extent that terminally differentiated cells acquire a post-mitotic state from which they can no longer re-enter the cell cycle. Moreover, the sensing of differentiation signals requires a lengthening of G1 phase, so that cell fate decisions are made before the cell is committed to a new round of division (reviewed in Dalton, 2015). In spite of quiescence and differentiation being different in many aspects, initiation of both processes relies on the sustained inactivation of cyclin-dependent kinase (CDK) complexes during G1, before the passage of the restriction point. Once this point has been traversed, cells engage in an autonomous program and are refractory to environmental signals. CDK inhibitors (CKIs) belonging to the CIP/KIP family (including p21, p27, and p57) are central players in the control of CDK activity during G1 and are essential during quiescence and differentiation (Zhang et al., 1999; Oesterle et al., 2011; Matsumoto et al., 2011). In particular, p21 restrains passage through the restriction point in the absence of mitogenic signaling and is critical to halt cell cycle progression in response to DNA damage (Deng et al., 1995; Barr et al., 2017, 2016; Heldt et al., 2018; Dulić et al., 1994).

In multicellular organisms quiescence serves the purposes of limiting growth, shaping the structure of tissues (O'Farrell, 2011), and protecting the stem cell niche (Cheung and Rando, 2013), whereas in unicellular systems, cell cycle exit is required to survive nutritional deprivation until better conditions arise. In the case of yeast cells, nitrogen starvation not only induces quiescence but also is the trigger for sexual differentiation, mating, and sporulation. Although the signals leading to cell cycle withdrawal in yeast and humans differ, the underlying mechanism for the arrest of cell cycle progression (CDK downregulation) is common to both systems. Hence, work in yeast might unveil new elements of control during quiescence that are also relevant in metazoans.

[1]Centre for Molecular Medicine Norway (NCMM), Nordic EMBL Partnership, University of Oslo, Oslo, Norway

[2]Department of Chemistry, University of Oslo, Oslo, Norway

[3]Department of Biosciences, University of Oslo, Oslo, Norway

[4]Both authors contributed equally

[5]Lead Contact

*Correspondence: r.m.martin@ncmm.uio.no (R.M.), sandra.lopez-aviles@ncmm.uio.no (S.L.-A.)

https://doi.org/10.1016/j.isci.2020.101063

In this regard, the fission yeast *Schizosaccharomyces pombe* has proved an excellent model to study cell cycle progression and its modulation by environmental cues. During growth under optimal conditions the *S. pombe* cell cycle is characterized by a very short G1 phase and a long G2 phase, when most of the growth occurs. However, when the surrounding medium is poor in nitrogen, the distribution of the cell cycle changes dramatically, with a shortening of G2 and the prolongation of G1. In the extreme case of the complete depletion of a source of nitrogen, fission yeast cells arrest their cell cycle progression in G1 phase, before the restriction point (Start in yeast). Upon this initial arrest, they become quiescent or, in the presence of a differentiation stimulus (that is, the presence of a mating partner), they undergo sexual differentiation. The continued repression of CDK activity (which in *S. pombe* is solely provided by the CDK1 homolog Cdc2) in this situation is critical for the engagement of the transcriptional differentiation program (Kjaerulff et al., 2007) and to prevent commitment to a new round of division.

In the core of this G1 arrest lies the only CKI in fission yeast, Rum1, and the anaphase-promoting complex/cyclosome (APC/C) activator Ste9. They cooperate in the inhibition of G1-S and M-phase CDK complexes and prevent further activation of the M-CDK complex through the targeted degradation of the mitotic cyclin Cdc13 (Correa-Bordes and Nurse, 1995; Stern and Nurse, 1998; Moreno and Nurse, 1994; Kominami et al., 1998b; Kitamura et al., 1998; Yamaguchi et al., 1997; Correa-Bordes, 1997). Of note, Rum1 and Ste9 are themselves counteracted by CDK-mediated phosphorylation (Benito et al., 1998; Blanco et al., 2000), and this regulation results in double-negative feedback loops that are instrumental for the bistable behavior of the system. Under rich conditions, phosphorylation of Rum1 leads to its degradation by the $SCF^{Pop1/Pop2}$ (Skp1-Cullin1-F-box) (Kominami et al., 1998a; Kominami and Toda, 1997), whereas phosphorylation of Ste9 hinders its binding to the APC/C. Altogether this facilitates a rapid increase in CDK activity that drives cells into S-phase. Under restrictive growth conditions, however, the balance is tilted toward Rum1 and Ste9, and this leads to cell-cycle arrest. Here, we investigate whether a protein phosphatase activity contributes to the initial activation of Rum1 and Ste9 that triggers cell cycle exit in fission yeast. By doing so, we reveal a pivotal role of PP2A-B56 enzymes counteracting CDK phosphorylation of Rum1 that has significant consequences for cell differentiation. We characterize their interaction and show that $PP2A\text{-}B56^{Par1}$ is essential for the timely accumulation of Rum1, CDK repression, and activation of Ste9 during the nitrogen starvation response. In addition, we find that this role can be extended to other situations that require stalling of cell cycle progression through G1 and therefore constitutes an important element of CDK control.

RESULTS

$PP2A\text{-}B56^{Par1}$ Activity Is Required for Cell-Cycle Arrest and Mating upon Nitrogen Deprivation

In fission yeast, the sexual differentiation response is closely linked to the sensing of nutritional deprivation that ultimately leads to CDK inhibition and the arrest of cell-cycle progression in G1. Therefore, we reasoned that if a protein phosphatase was required for the sustained downregulation of CDK activity at the end of the cell cycle, its loss would also affect the G1 arrest and mating response. To address this possibility, we investigated the mating efficiency upon nitrogen depletion (calculated as the proportion of zygotes and tetrads present in a homothallic culture) of mutants of the Cdc14-type phosphatase Clp1, of PP1, and of PP2A. PP2A enzymes are multimeric complexes containing a scaffolding A subunit, a catalytic C subunit, and a variable regulatory B subunit, which provides specificity to the complex (Janssens et al., 2008). Hence, we decided to use in our analysis mutants of the two main regulatory subunits of PP2A: *pab1* (corresponding to B55) and *par1* (the major B56 subunit). A second (minor) B56 subunit, Par2, also contributes to PP2A-B56 activity in the cell. However, its loss does not produce noticeable phenotypic defects in a wild-type (WT) background and only has consequences when combined with the deletion of *par1* (Jiang and Hallberg, 2000). Therefore, we did not include the individual *par2* mutant in our initial analysis.

In the case of PP1 we analyzed the behavior of the deletion mutant of the major catalytic subunit, Dis2. This mutant and the *clp1* mutant did not show any mating defect (*clp1*Δ cells responded even faster than the WT control strain), whereas PP2A mutants behaved differently. Our group had previously shown that loss of *pab1* results in exacerbated conjugation (Martín et al., 2017). Strikingly, in the absence of Par1, fission yeast cells depicted a delayed mating response and their overall mating ability was reduced compared with the rest of the strains analyzed (Figures 1A and 1B). This defect correlated with the impaired induction of the master regulator of meiosis *mei2* (Figure S1A) and the reduced phosphorylation of the pheromone-sensing MAPK Spk1 (Figure S1B). This was not the consequence of defective sensing of the nitrogen depletion,

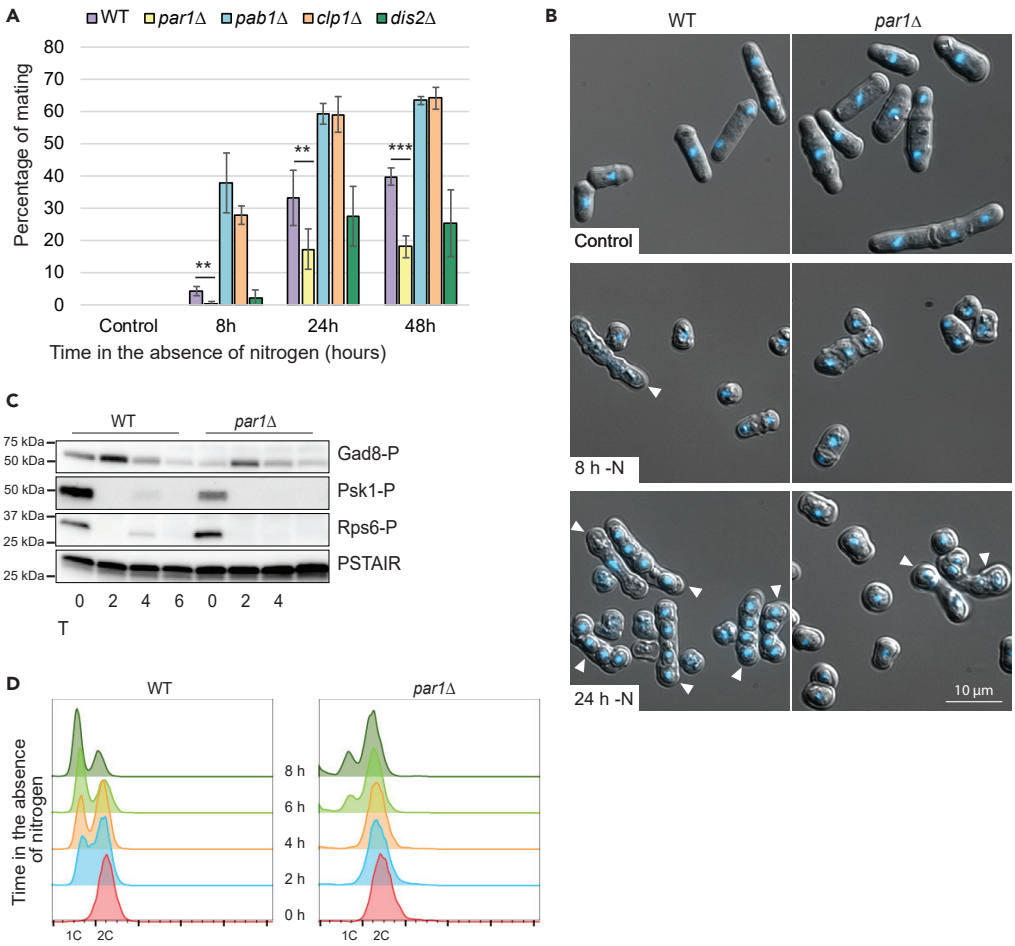

Figure 1. PP2A-B56^{Par1} Activity Is Required for an Adequate Mating and Cell-Cycle Arrest in G1 upon Nitrogen Depletion

(A) Homothallic WT, *pab1*Δ, *par1*Δ, *clp1*Δ, and *dis2*Δ cells were incubated at 25°C in the absence of nitrogen, and their mating ability was determined at 0, 8, 24, and 48 h. Mean values of five biological replicates ± SD are shown. Statistical significance of the difference between strains was assessed with a t test assuming two-tailed distribution and unequal variance. **p < 0.01, and ***p < 0.001.

(B) Homothallic WT and *par1*Δ cells were maintained at 25°C in the absence of nitrogen. Cells were fixed at indicated time points, and pictures were taken after staining the cells with DAPI. Differential interference contrast images were overlaid to determine the cell outline. Arrowheads indicate zygotes and tetrads.

(C) Homothallic WT and *par1*Δ cells were incubated at 25°C in the absence of nitrogen, and samples were collected at the indicated time points. Phosphorylation at Ser546 of the AKT homolog Gad8 was used as a readout of TORC2 activity. Phosphorylation of Psk1 (S6 kinase in *S. pombe*) and Rps6 (ribosomal protein S6) were used as a readout of the activity of TORC1, and total Cdc2 (PSTAIR) served as loading control.

(D) Flow cytometric analysis of the DNA content of isolated nuclei from heterothallic WT and *par1*Δ cells collected at the indicated time points during a time course in the absence of nitrogen.

See also Figure S1.

because TORC1 inactivation and TORC2 activation occurred normally (Figure 1C). Rather the mating defect correlated with the inability of *par1*Δ cells to halt cell-cycle progression in G1 (Figure 1D). Hence, these results suggest that PP2A-B56^{Par1} is required for the cell-cycle arrest that precedes the sexual differentiation response in fission yeast.

Loss of PP2A-B56^{Par1} Impairs the Degradation of Cdc13 (CycB)

The cell-cycle defect in *par1*Δ cells could be due to alterations in the kinetics of CDK activity in response to nitrogen starvation. To investigate this possibility we analyzed the levels of the S-phase cyclin Cig2 and the

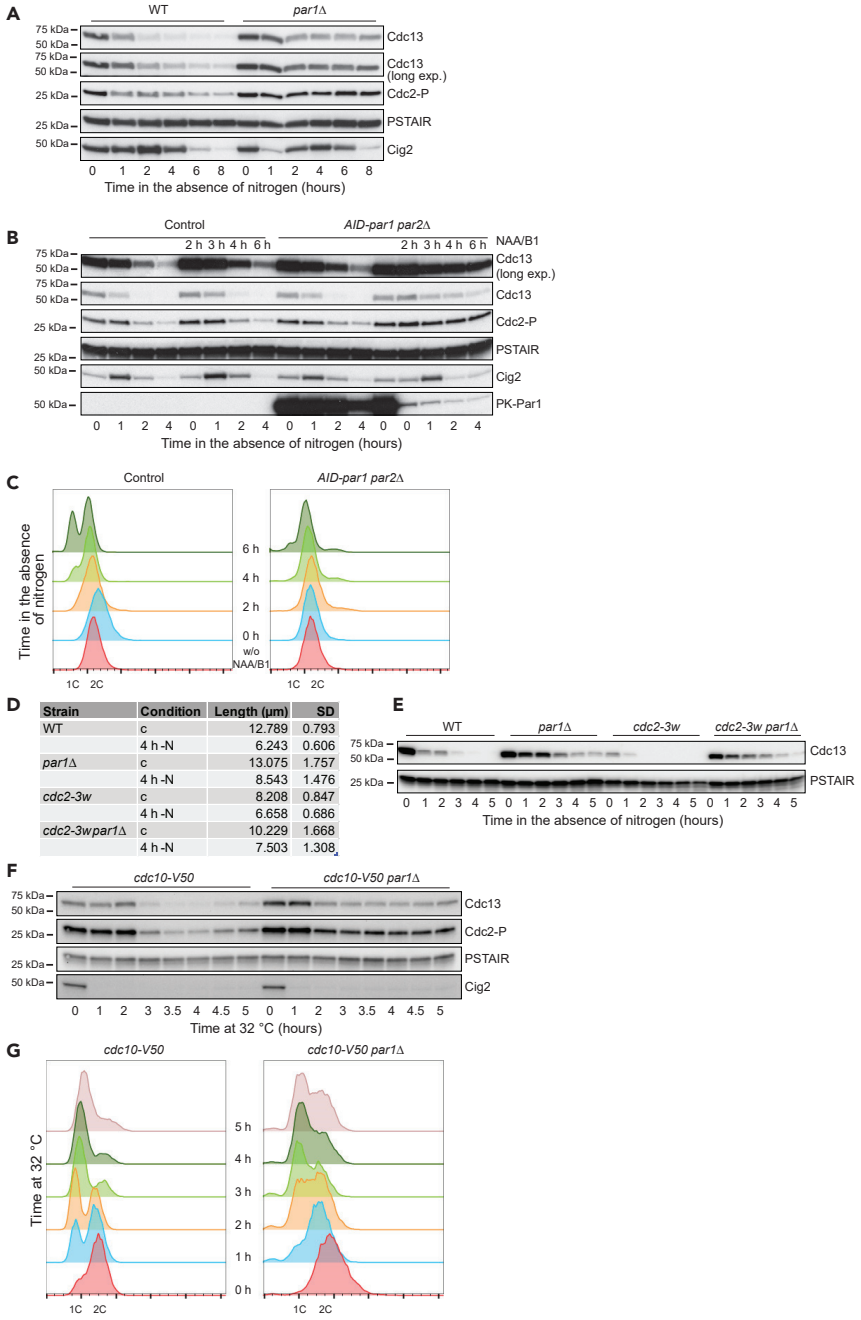

Strain	Condition	Length (μm)	SD
WT	c	12.789	0.793
	4 h -N	6.243	0.606
par1Δ	c	13.075	1.757
	4 h -N	8.543	1.476
cdc2-3w	c	8.208	0.847
	4 h -N	6.658	0.686
cdc2-3w par1Δ	c	10.229	1.668
	4 h -N	7.503	1.308

Figure 2. Depletion of Par1 Activity Prevents the Complete Degradation of Cdc13

(A) Homothallic WT and *par1***Δ** cells were incubated at 25°C in the absence of nitrogen, and samples were collected at the indicated time points. Protein levels of Cdc13, Cig2, and phosphorylation of Cdc2 on Tyr15 were followed over the time course by western blot. Total Cdc2 (PSTAIR) served as loading control.

(B) Control cells containing the auxin-inducible degron background (*Padh15-skp1-At-Tir1-2NLS Padh15-sk1-Os-Tir1*) and *nmt41-3PK-miniAID-par1 par2***Δ** cells in the same genetic background (referred to as *AID-par1 par2***Δ**) were treated or not (as indicated in the figure) with thiamine (0.5 μM) and 1-Naphthaleneacetic acid potassium salt (NAA; 1 mM) 2 h before being incubated in the absence of nitrogen. Samples were collected at the indicated time points. Protein levels of Cdc13 and Cig2, and phosphorylation of Cdc2 on Tyr15, were determined by western blot. $B56^{Par1}$ depletion was assessed by western blot against its N-terminal 3PK tag. Total Cdc2 (PSTAIR) was used as loading control.

(C) Flow cytometric analysis of the DNA content of control cells containing the auxin-inducible degron background (*Padh15-skp1-At-Tir1-2NLS Padh15-sk1-Os-Tir1*) and *nmt41-3PK-miniAID-par1 par2***Δ** treated or not with thiamine

Figure 2. *Continued*
(0.5 μM) and NAA (1 mM) and collected at the indicated time points during a time course in the absence of nitrogen. At least 7,000 gated single nuclei are represented at each time point.
(D) Heterothallic h-WT, *par1*Δ, *cdc2-3w,* and *cdc2-3w par1*Δ cells were incubated at 30°C in EMM (control) or in EMM-N for 4 h. Fixed cells were measured after staining them with Calcofluor.
(E) Heterothallic h-WT, *par1*Δ, *cdc2-3w,* and *cdc2-3w par1*Δ cells were incubated at 30°C in the absence of nitrogen, and samples were collected at the indicated time points. Protein levels of Cdc13 were assessed by western blot. Total Cdc2 (PSTAIR) was used as loading control.
(F) *cdc10-V50* and *cdc10-V50 par1*Δ cells were incubated at 32°C for the indicated time. Control cells were incubated at 25°C. Western blots show Cdc13 and Cig2 levels, phosphorylation of Cdc2, and total Cdc2 (PSTAIR) as loading control.
(G) Flow cytometric analysis of the DNA content of isolated nuclei from *cdc10-V50* and *cdc10-V50 par1*Δ cells collected at the indicated time points during a time course at 32°C.
See also Figure S2.

mitotic cyclin Cdc13 (both of them B-type cyclins; Fisher and Nurse, 1995) in a WT and a *par1*Δ strain. As expected, in the WT background nitrogen deprivation led to a sudden and sustained drop in the levels of Cdc13, which was almost undetectable after 2 h of treatment (Figure 2A). Cig2 behaved differently, increasing slightly during the initial time points and then dropping steadily until its complete disappearance after 6–8 h of starvation (when a majority of the cells were already arrested in G1). In contrast, in the *par1*Δ mutant, Cdc13 showed an initial decrease, but then it remained stable for the remainder of the experiment (Figure 2A). Cig2 levels were closer to those of the WT strain, and we could only observe a small delay in its disappearance that affected the last time point of our time course. We also determined the presence of Cdc2-Tyr15 phosphorylation in our cells. This conserved inhibitory phosphorylation occurs as the Cdc2-Cdc13 complex is being formed to prevent its premature activation during G2 phase, and it is only removed during mitosis to allow full activation of the complex (Parker et al., 1992; Gould and Nurse, 1989). In addition, the G1-S CDK complex Cdc2-Cig2 is also phosphorylated when DNA replication is halted, and this prevents mitotic entry in the presence of unreplicated DNA (Zarzov et al., 2002). In G1-arrested cells this mark nearly disappeared, because the low level of Cdc13 limits the formation of the Cdc2-Cdc13 complex, which is a prerequisite for its phosphorylation (Figure 2A). Nevertheless, a low level of phosphorylation remained, and this has been previously suggested to be important during the nitrogen starvation response (Wu and Russell, 1997). In agreement with the defective cell-cycle arrest and continuous presence of Cdc13 in *par1*Δ cells, Tyr15 phosphorylation was detectable throughout the time course, indicating the prevalence of G2 cells in this strain.

The same defects in Cdc13 degradation and Tyr15 phosphorylation dynamics were clear when we used a conditional mutant of *par1* in a *par2*Δ background (*nmt41-miniAID-par1 par2*Δ, where Par1 is fused to a 68-amino acid fragment of the Auxin-Inducible Degron AID/IAA17) and we depleted Par1 only 2 h before the nitrogen starvation treatment (Figure 2B). Similar to the *par1*Δ mutant, these cells also failed to arrest their cell-cycle progression in G1 (Figure 2C). Thus, we were confident that this was a *bona fide* defect due to the loss of *par1* and not the consequence of reduced fitness in cells lacking PP2A-B56^{Par1} activity over many generations.

Accelerated mitotic entry and the subsequent cell size reduction in response to nitrogen deprivation contribute to the cell-cycle arrest in G1, because cells that have not satisfied the size requirement to enter S-phase will delay the G1/S transition (what is known as the *G1 cell size control or checkpoint*; Novak et al., 1998). We observed that *par1*Δ cells have a slightly longer generation time than WT cells (5 h 20 min versus 4 h 30 min at 25°C in Edinburgh minimal medium (EMM)). Therefore, we wanted to rule out that the G1 arrest and Cdc13 degradation defect in *par1*Δ cells was not merely due to a longer residence time in the G2 phase of the cell cycle or to their inability to accelerate mitotic entry and engage the G1 cell size checkpoint. To this end, we combined the *par1* deletion with a gain-of-function mutation of the *cdk1/cdc2* gene (the *cdc2-3w* allele) (Fantes, 1981; Enoch and Nurse, 1990). On its own, the presence of this allele results in a decrease in cell length compared with cells containing the WT gene (indicative of premature mitotic entry). The double mutant *par1*Δ *cdc2-3w* was shorter than the WT control (Figure 2D). However, this size reduction only marginally ameliorated the Cdc13 degradation defect in response to nitrogen starvation (Figure 2E). We obtained a similar result when we introduced the *cdc25-9A* allele in the *par1*Δ background. This allele, mutated in the phosphorylation sites for the checkpoint and stress kinases Cds1, Chk1, and Srk1 (Zeng et al., 1998; Lopez-Aviles et al., 2005), is immune to the cell-cycle arrest in G2 imposed by activation of the DNA and replication checkpoints and in response to stress. Therefore, we excluded the possibility that a slower transit through G2 due to checkpoint activation was responsible for the retention

of Cdc13 in the *par1*Δ mutant (Figure S2A). Given the role of PP2A-B56^{Par1} in the silencing of the spindle assembly checkpoint (SAC) (reviewed in Saurin, 2018; Hayward et al., 2019), we also analyzed the degradation of Cdc13 during nitrogen starvation in the *par1*Δ mutant in the absence of the SAC component Mad2. As in the previous cases, this experiment showed that persistent SAC signaling was not the reason for the retention of Cdc13 in nitrogen-starved *par1*Δ cells (Figure S2B).

Together, these results indicate that the persistence of Cdc13 in *par1*Δ cells during G1 phase cannot be merely due to defects in the G2 and M phases of the previous cycles but is the result of additional elements of control of the mitotic cyclin being altered in this strain.

Confirming this idea, *par1*Δ cells also failed to degrade Cdc13 when a G1 arrest was imposed through the inactivation of the MBF transcription factor Cdc10 using a *cdc10-V50* allele at restrictive temperature (Figure 2F). In contrast to the nitrogen starvation response, the G1 arrest in this mutant does not require a premature entry into mitosis or the engagement of the G1 cell size checkpoint. Of note, the inability of the *par1*Δ mutant to fully degrade Cdc13 was accompanied by a failure to sustain the G1 arrest in this mutant (Figure 2G), a phenotype also observed in *ste9*-deleted cells (Kitamura et al., 1998). Therefore, we conclude that PP2A-B56^{Par1} activity is required to prevent the passage through Start (the point after which the cell is committed to a new round of division), and this is achieved through the regulation of the degradation of the mitotic cyclin Cdc13.

Deletion of the G1/S Cyclins Rescues the Defects in Cdc13 Degradation and G1 Arrest of par1Δ Cells

Given that *par1*Δ cells cannot efficiently arrest their cell cycle in G1 or degrade the mitotic cyclin in response to nitrogen starvation we decided to test whether this defect could be rescued by a decrease in the G1/S CDK activity. For this aim we deleted the genes encoding the G1/S cyclins Cig1 and Cig2. This strategy has been previously used to rescue the mating and cell-cycle arrest defects in strains that fail to counteract CDK activity upon nitrogen depletion, such as those containing mutant alleles of *wee1*, *ste9*, and *rum1* (Wu and Russell, 1997; Kitamura et al., 1998; Martín-Castellanos et al., 1996). These rescues can be understood as the consequence of canceling out the double-negative feedback loops established between CDK complexes and CDK antagonists.

The deletion of *cig1* and *cig2* does not have a noticeable impact on the cell-cycle distribution of cells growing exponentially in rich medium (Fisher and Nurse, 1996; Mondesert et al., 1996). However, it facilitates the G1 arrest upon nitrogen depletion (Figure 3A, left lower panel). Consequently, the *cig1*Δ *cig2*Δ mutant has a higher mating efficiency and degrades Cdc13 more readily than its WT counterpart (Figures 3B–3D). Deletion of *cig1* and *cig2* in the *par1*Δ background completely suppressed the G1 arrest and mating defects of the single *par1*Δ mutant (Figure 3A, right lower panel, 3B and 3D). Remarkably, the triple mutant *par1*Δ *cig1*Δ *cig2*Δ degraded Cdc13 with faster kinetics than the WT strain (Figure 3C). In contrast, individual deletions of either *cig1* or *cig2* resulted in a partial rescue of the Cdc13 degradation defect observed in *par1*Δ cells (Figures S3A and S3B). Of the two cyclins, however, Cig2 appeared to have a more prominent role because its deletion in the *par1*Δ mutant mirrored the behavior of the WT control. Altogether, these findings indicated that PP2A-B56^{Par1} is important to counteract CDK activity in G1, and therefore we were compelled to investigate its involvement in the regulation of CDK inhibitors.

The Cdc13 Degradation Defect of *par1*Δ Cells Correlates with Their Inability to Dephosphorylate Ste9 and Stabilize Rum1

Cdc13 degradation during G1 requires the APC/C activator Ste9 (Kitamura et al., 1998; Blanco et al., 2000; Yamaguchi et al., 1997; Kominami et al., 1998b) and the CKI Rum1 (Correa-Bordes, 1997). Both these CDK-negative regulators are themselves inhibited by CDK-dependent phosphorylation, which leads to dissociation from the APC/C of the former and targeted degradation of the latter (Blanco et al., 2000; Benito et al., 1998).

The cooperation between these two CDK inhibitors is patent during the nitrogen starvation response (and other events leading to G1 arrest), as deletion mutants of either *ste9* or *rum1* fail to degrade Cdc13 (Figures S4A and S4B).

As the *par1*Δ mutant is comparably defective in downregulating Cdc13, and given the regulation by phosphorylation of both Ste9 and Rum1, we next tested the ability of *par1*Δ cells to dephosphorylate and stabilize them, respectively, upon nitrogen depletion. Ste9 dephosphorylation can be observed in G1-arrested cells or when CDK activity is exogenously abrogated. Conversely, it becomes phosphorylated

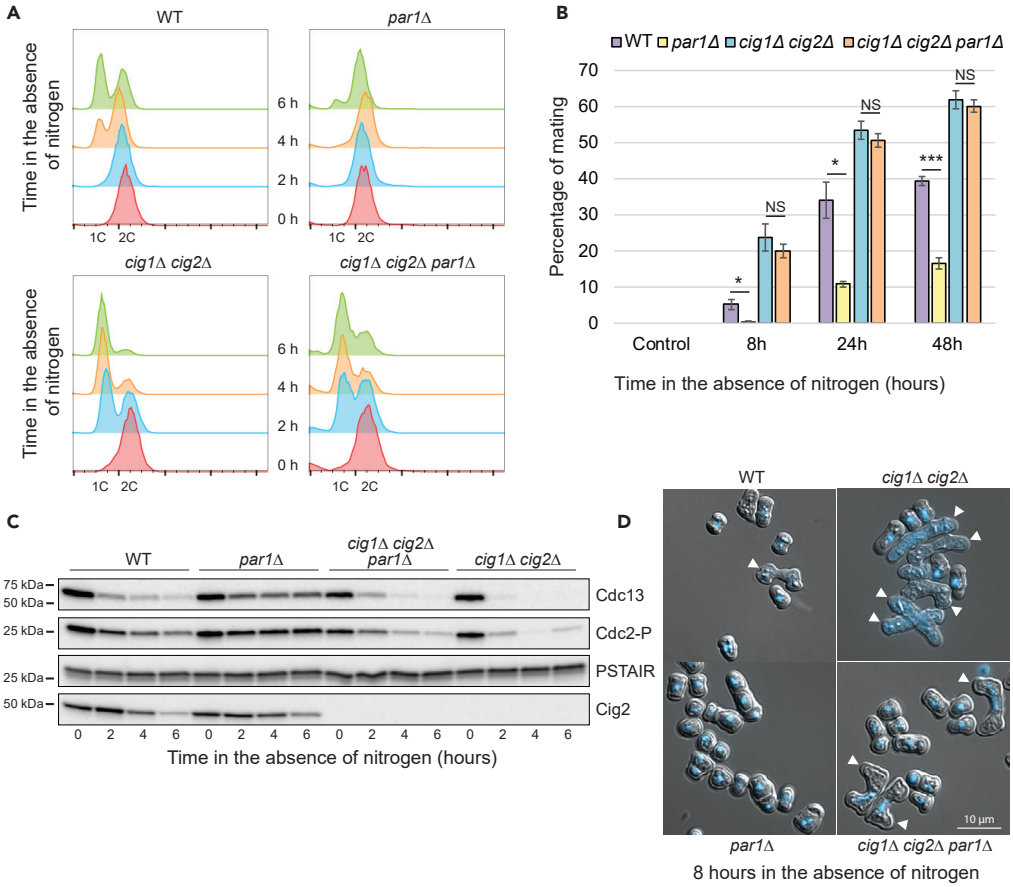

Figure 3. Rescue of the Defect in the G1 Arrest, Mating Efficiency, and Degradation of Cdc13 of a *par1*Δ Mutant by Deletion of the G1/S Cyclins

(A) Homothallic WT, *par1*Δ, *cig1*Δ *cig2*Δ, and *cig1*Δ *cig2*Δ *par1*Δ cells were incubated at 25°C in the absence of nitrogen; cells were collected at the indicated time points, and after processing their DNA content was measured by flow cytometry.

(B) Efficiency of mating of the homothallic strains WT, *par1*Δ, *cig1*Δ *cig2*Δ, and *cig1*Δ *cig2*Δ *par1*Δ after 0, 8, 24, and 48 h upon nitrogen depletion. Mean values of three biological repeats ± SD are shown. Statistical significance of the difference between strains was assessed with a t test assuming two-tailed distribution and unequal variance. *$p < 0.05$, ***$p < 0.001$.

(C) Homothallic WT, *par1*Δ, *cig1*Δ *cig2*Δ, and *cig1*Δ *cig2*Δ *par1*Δ cells were incubated at 25°C in the absence of nitrogen, and samples were collected at the indicated time points. Protein levels of Cdc13 and Cig2 and phosphorylation of Cdc2 on Tyr15 were assessed by western blot. Total Cdc2 (PSTAIR) served as loading control.

(D) Homothallic WT, *par1*Δ, *cig1*Δ *cig2*Δ, and *cig1*Δ cig2Δ *par1*Δ cells were maintained in the absence of nitrogen for 8 h. Pictures of fixed cells were taken after staining them with DAPI. Differential interference contrast images were overlaid to determine the cell outline. Arrows indicate zygotes.

See also Figure S3.

during S, G2, and M phases, as CDK activity increases (Blanco et al., 2000, and Figure S4D). These two states can be discerned based on the different electrophoretic mobility of the phosphorylated versus non-phosphorylated protein (Figure S4D). In WT cycling cells, only the phosphorylated form was detected. However, upon nitrogen starvation, an additional, faster-migrating band corresponding to the non-phosphorylated form of Ste9 started to appear 2 h within the treatment and gained intensity as more cells accumulated in G1 (Figures 4A, 7D, S4D, and S4E). In contrast, in the *par1*Δ strain the slower-migrating band (indicative of phosphorylation) was more prominent throughout the entire time course, and the faster-migrating band was barely present (Figures 4A, S4D, and S4E). Remarkably, we could observe the same behavior in a *rum1*Δ mutant (Figure S4E). In parallel to Ste9 dephosphorylation, the level of Rum1 started to increase in the WT strain 2 h within the experiment. However, *par1*Δ cells failed to show a significant accumulation of Rum1 over the 6-h time course (Figure 4B). This was not the consequence of reduced transcription of

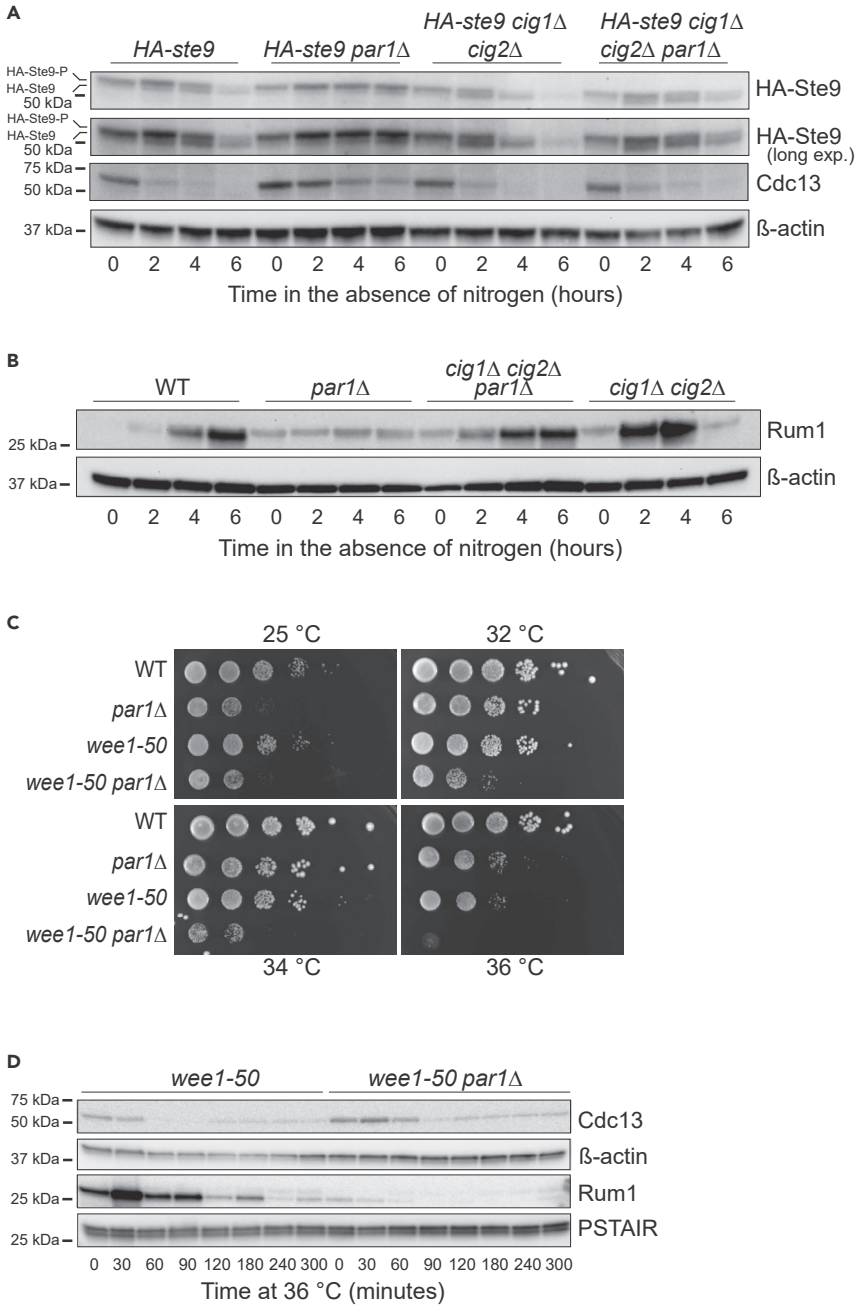

Figure 4. Deletion of *par1* Causes a Defect in Ste9 Dephosphorylation and Rum1 Stabilization

(A) Homothallic *HA-ste9*, *HA-ste9 par1*Δ, *HA-ste9 cig1*Δ *cig2*Δ, and *HA-ste9 cig1*Δ *cig2*Δ *par1*Δ cells were incubated at 25°C in the absence of nitrogen, and samples were collected at the indicated time points. Protein levels of Cdc13 were followed over the time course by western blot. Ste9 was detected by western blot against its N-terminal HA-tag. β-Actin served as loading control. HA, hemagglutinin.

(B) Homothallic WT, *par1*Δ, *cig1*Δ *cig2*Δ, and *cig1*Δ *cig2*Δ *par1*Δ cells were incubated at 25°C in the absence of nitrogen, and samples were collected at the indicated time points. Protein levels of Rum1 were assessed by western blot. β-Actin was used as loading control.

(C) WT, *par1*Δ, *wee1-50*, and *wee1-50 par1*Δ cells were grown in liquid rich medium (yeast extract with supplements (YES)) medium at 30°C and then spotted onto YES plates at serial 10-fold dilutions (from left to right). Plates were incubated at 25°C, 32°C, 34°C, and 36°C for 3 days before pictures were taken.

Figure 4. *Continued*

(D) *wee1-50* cells and *wee1-50 par1*Δ cells were incubated at 36°C, and samples were collected at the indicated time points. Control cells (0 time point) were incubated at 25°C. Western blots show protein levels of Cdc13, Rum1 together with β-actin and Cdc2 (PSTAIR) as loading controls. See also Figure S4.

rum1 in this mutant, because *rum1* mRNA was induced to comparable levels in both strains (Figure S4C). Notably, loss of *cig1* and *cig2* utterly overrode these defects, pointing at PP2A-B56^{Par1} as the phosphatase in charge of counteracting CDK phosphorylation on Rum1 and Ste9 (Figures 4A and 4B).

Finally, indicating that this regulation was not exclusive of the nitrogen starvation response, we observed a genetic interaction between the *par1* deletion and the *wee1-50* allele (Figure 4C). *wee1-50* cells have a shorter G2 phase, which results in premature mitosis (Russell and Nurse, 1987), an effect that is exacerbated with temperature. To avoid the progressive shortening of the cell, this mutant expands the G1 phase, a process that requires Rum1 and Ste9 activities. In their absence, *wee1-50* cells become shorter in every cycle, eventually losing their viability (Moreno and Nurse, 1994; Correa-Bordes and Nurse, 1995). Deletion of *par1* also affected the survival of the *wee1-50* mutant (Figure 4C), and this worsening of the phenotype correlated with the inability of the double *wee1-50 par1*Δ mutant to accumulate Rum1 (Figure 4D).

All in all, these results suggest that PP2A-B56^{Par1} is an important regulator of the CDK inhibitors Ste9 and Rum1 and that this regulation is instrumental for the arrest in G1 phase that precedes differentiation and during other special cell cycles that require an expansion of G1.

Overexpression of a PP2A-B56-Specific Small Linear Motif (SLiM) Decoy Phenocopies the Deletion of *par1*

The aforementioned results strongly suggested that Rum1 and Ste9 are targets of PP2A-B56^{Par1}. PP2A-B56 enzymes recognize a small linear interacting motif (SLiM) found in disordered regions of their substrates (LxxIxE) (Wang et al., 2016; Hertz et al., 2016). To address whether the effects that we had observed upon deletion of *par1* were due to the inability of the complex to interact with its substrates we overexpressed a peptide encompassing the optimal sequence of this motif (LEPIPEEPE, based on the RepoMan SLiM and fused to GFP for convenience) (Figure S5). A similar strategy has been used before to prevent the recognition of PP2A-B56 specific targets (Kruse et al., 2018). This construct (Par1-inhibitor, referred to as GFP-B56-SLiM hereafter) expressed from the strong *nmt1* promoter was able to recapitulate the phenotype of the *par1*Δ mutant after 24 h of overexpression (Figure 5A), indicating that it could outcompete PP2A-B56 canonical substrates. Indeed, the cell separation defect typical of *par1*Δ cells was accentuated in cells expressing the Par1-inhibitor for longer times (Figure 5A), which was reminiscent to the complete loss of B56 activity upon depletion of both Par1 and Par2 (Jiang and Hallberg, 2000). As a control, we overexpressed a mutated version of the Par1-inhibitor where the key residues I_4 and E_6 had been mutated to Ala (mock-inhibitor, referred to as GFP-B56-SLiM-AA). As expected, this mutant peptide failed to efficiently bind Par1 and to produce a similar phenotype (Figures 5A and 5B). In agreement with our hypothesis, overexpression of the Par1-inhibitor, but not the mock-inhibitor, impaired the degradation of Cdc13 to an extent similar to the *par1* deletion (Figure 5C). Therefore, we conclude that overexpression of the Par1-inhibitor can be used as an alternative to the deletion mutant in the analysis of PP2A-B56^{Par1} phenotypes. More importantly, these results indicate that the defects observed in the *par1*Δ mutant are due to the inability of PP2A to interact with B56-specific substrates.

PP2A-B56^{Par1} Interacts with Rum1 *In Vitro*

Having delineated the phenotypes upon loss of PP2A-B56^{Par1} in relation with Rum1 and Ste9, we asked whether they interact. We started by using a linear-motif prediction tool (ELM) (Gouw et al., 2018) to determine putative SLiMs present in Rum1 and Ste9 that could mediate their interaction with PP2A-B56^{Par1}. Analysis of their sequences showed that whereas Ste9 does not contain an obvious PP2A-B56-SLiM that adheres to the strict consensus, Rum1 comprises two potential PP2A-B56-SLiMs. These two motifs (^{39}IDEIPE^{44} and ^{80}LERCMEE^{86}) surround the two main phospho-sites targeted by CDK (T58 and T62) (Benito et al., 1998) (Figure 6A).

Following this sequence analysis, we wanted to analyze the interaction between PP2A-B56^{Par1} Rum1 and Ste9. Neither Rum1 nor Ste9 are abundant proteins, which hampers their purification from yeast native extracts. Hence, to test whether Par1 and Ste9/Rum1 directly interact we expressed and purified Rum1 and Ste9 from *E. coli*, and the recombinant proteins were subsequently incubated with TAP-tagged Par1 pulled down from fission yeast. As anticipated from the motif analysis, Ste9 binding to Par1 was very weak

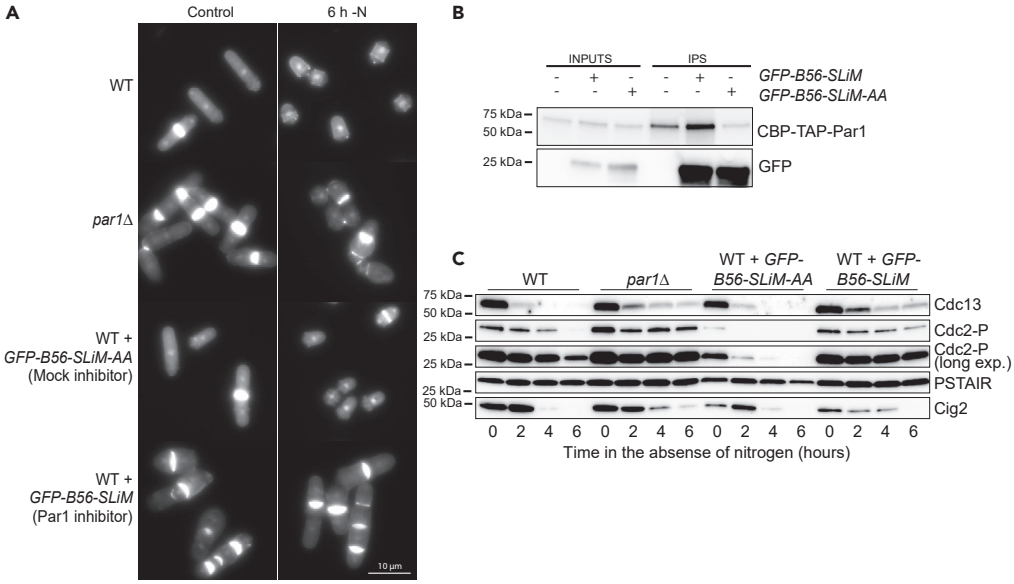

Figure 5. The Defect in the Degradation of Cdc13 in a *par1*Δ Mutant Is Due to Inability of PP2A to Interact with B56-Specific Substrates

(A) WT and *par1*Δ cells, and WT cells transformed with either pREP1-GFP-B56-SLiM-AA (mock-inhibitor) or pREP1-GFP-B56-SLiM (Par1-inhibitor), were incubated in EMM in the absence of thiamine for 40 h at 25°C. Subsequently, cells were shifted to fresh EMM (control point) and to EMM-N for 6 h. Cells were fixed and stained with DAPI and Calcofluor before obtaining images.

(B) Overexpressed GFP-B56-SLiM (Par1-inhibitor) and GFP-B56-SLiM-AA (mock-inhibitor) were purified by means of their N-terminal GFP-tag using a GFP trap from cells containing a TAP-tagged allele of *par1*. A representative experiment shows the co-purifying and the unspecifically pulled down TAP-Par1 detected through western blot against the CBP epitope in the TAP-tag. Western blot against GFP served as control of the GFP pull down.

(C) WT and *par1*Δ cells, and WT cells transformed with either pREP1-GFP-B56-SLiM-AA (mock-inhibitor) or pREP1-GFP-B56-SLiM (Par1-inhibitor) were incubated in EMM in the absence of thiamine for 40 h at 25°C. Cells were shifted to EMM-N, and samples were collected at the indicated time points. Western blots show protein levels of Cdc13 and Cig2, phosphorylation of Cdc2 on Tyr15, and total Cdc2 (PSTAIR) as loading control. See also Figure S5.

(Figure 6B), whereas the interaction between Par1 and Rum1 was much stronger (Figure 6C). The same result was obtained when immobilized Rum1 was incubated with TAP-Par1-containing extracts (Figure S6). Moreover, when we incubated Rum1 with TAP-Par1 containing a mutation in one of the residues in the binding pocket previously shown to be critical for the recognition of the LxxIxE motif (Hertz et al., 2016) (TAP-Par1F314Q), this interaction was reduced (Figure 6C). Therefore, we conclude that Rum1 is the most likely a direct substrate of PP2A-B56^{Par1}. Given that Rum1 is needed for counteracting CDK activity during G1, these results support a scenario where PP2A-B56^{Par1} dephosphorylates and stabilizes Rum1, leading to a drop in CDK activity that ultimately results in the activation of the APC/C^{Ste9}.

Mutation of *rum1* Putative B56 Binding Motif Phenocopies the *par1*Δ Mutant

If dephosphorylation of Rum1 by PP2A-B56^{Par1} is a requirement for its stabilization during G1, then hindering the interaction between the two proteins should lead to a phenotype comparable to that of the *par1*Δ mutant. To test this idea, we replaced the WT *rum1* gene by a mutant allele containing two alanine substitutions at positions 42 and 44, corresponding to the central I and E in the first SLiM (hereon referred to as *rum1 BM1AA* for *Binding Motif 1 I42A E44A*). Mutation of these residues led to a decrease in the mating efficiency comparable to the decrease observed in the *par1*Δ mutant (Figure 7A). In addition, *rum1 BM1AA* mutant cells were delayed in the G1 arrest following nitrogen starvation and in the degradation of Cdc13 (Figures 7B, 7C, S7A, and S7B). More importantly, this mutant failed to accumulate Rum1 in the cell, even though the mRNA levels were similar to those of the WT strain (Figure S7C) Finally, these observations correlated with a delay in the dephosphorylation of Ste9 (Figure 7D). Of note, concomitant mutation of the second putative binding motif (*BM2AA*) did not worsen the phenotype of the *rum1 BM1AA* mutant, but it actually ameliorated its defects (data not shown). Currently, we are missing structural insight

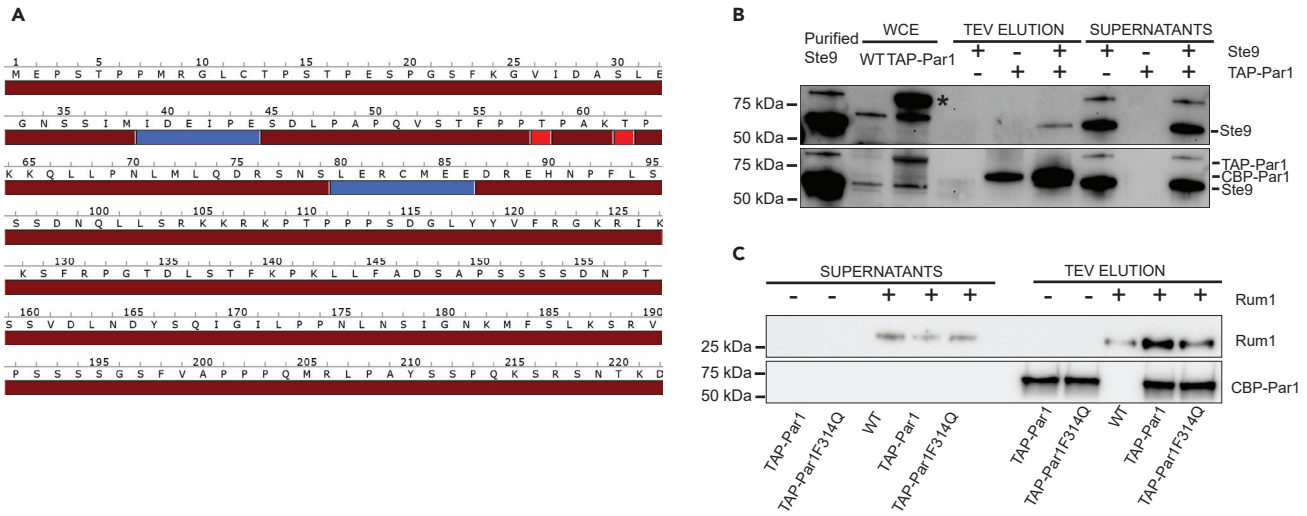

Figure 6. PP2A-B56 ^{Par1} Interacts with the CDK Inhibitor Rum1

(A) Amino acid sequence of Rum1. The putative SLiMs for PP2A-B56 are in blue and the sites phosphorylated by CDK are in red.

(B) TAP-Par1 was purified using the tandem affinity purification method. 100 ng of Ste9 homogeneous recombinant protein was added to the purified Par1, and after washing and eluting CBP-Par1 with TEV protease (which cleaves the TEV site between the protein A and CBP moieties of the TAP-tag), the bound (elution) and unbound (supernatants) Ste9 was detected by western blot. Untagged WT extract was used as a negative control. Note that, as Ste9 and Par1 have very similar molecular masses, and the protein A present in the TAP-tag is also bound by the rabbit IgGs, signal corresponding to the uncleaved TAP-Par1 appears in the Ste9 blot (marked with an asterisk). In the lower panel, signal coming from the previous incubation with the Ste9 antibody remains in the CBP western blot.

(C) TAP-Par1 and TAP-Par1F314Q were purified using the tandem affinity purification method. 50 ng of Rum1 homogeneous recombinant protein was added to the purified Par1 and TAP-Par1F314Q; after washing and eluting CBP-Par1 with TEV protease, the unbound (supernatants) and the interacting and unspecifically pulled down (elution) Rum1 was detected by western blot. Untagged WT extract was used as a negative control. The amount of pulled down CBP-Par1 and CBP-Par1F314Q were detected by western blot against the CBP-tag.

See also Figure S6.

into how this second mutation could affect Rum1 functionality and/or stability, and we have not tested the phenotype of the single *rum1 BM2AA* mutant. However, our results suggest that the first binding motif is sufficient for the interaction with PP2A-B56^{Par1}.

If PP2A-B56^{Par1}-mediated dephosphorylation of Rum1 is an important step for the downregulation of CDK activity during G1, an expected outcome of this model would be that expression of a phospho-null allele (*rum1-T58AT62A*) can rescue the Cdc13 degradation defect of a *par1*Δ mutant. Indeed, expression of this allele from the *nmt81* promoter was sufficient to fully restore the degradation of Cdc13 in *par1*Δ cells (Figure 7E).

All in all, these observations lead us to the conclusion that PP2A-B56^{Par1} is the phosphatase in charge of counteracting CDK activity during G1 phase establishment in fission yeast and that this role is mainly executed through the dephosphorylation of the CKI Rum1. These results are summarized in our model (Figure 8).

DISCUSSION

In all organisms, cell cycle progression has to be closely coordinated with the sensing of nutritional cues and pro-growth signaling. Even though the cell uses specific mechanisms to sense different perturbations or signals (be it environmental insults or nutritional scarcity) they all converge in the regulation of CDK activity, which ultimately dictates the quiescence/proliferation decision. In later years different protein phosphatases (Cdc14, PP1, PP2A) have been shown to play prominent roles in the regulation of cell cycle transitions by counteracting CDK-dependent phosphorylation events and the amplification of CDK activity (Stegmeier and Amon, 2004; Bouchoux and Uhlmann, 2011; Godfrey et al., 2017; Wu et al., 2009; Mochida et al, 2009, 2010; Gharbi-Ayachi et al., 2010; Schmitz et al., 2010; Mayer-Jaekel et al., 1994; Manchado et al., 2010; Grallert et al., 2015). In this study we have used the fission yeast response to nitrogen starvation to investigate the involvement of protein phosphatases in the downregulation of CDK activity during the pre-Start G1 arrest that precedes sexual differentiation. By doing so, we revealed an outstanding role of PP2A-B56^{Par1} in the control of CDK activity during G1 phase.

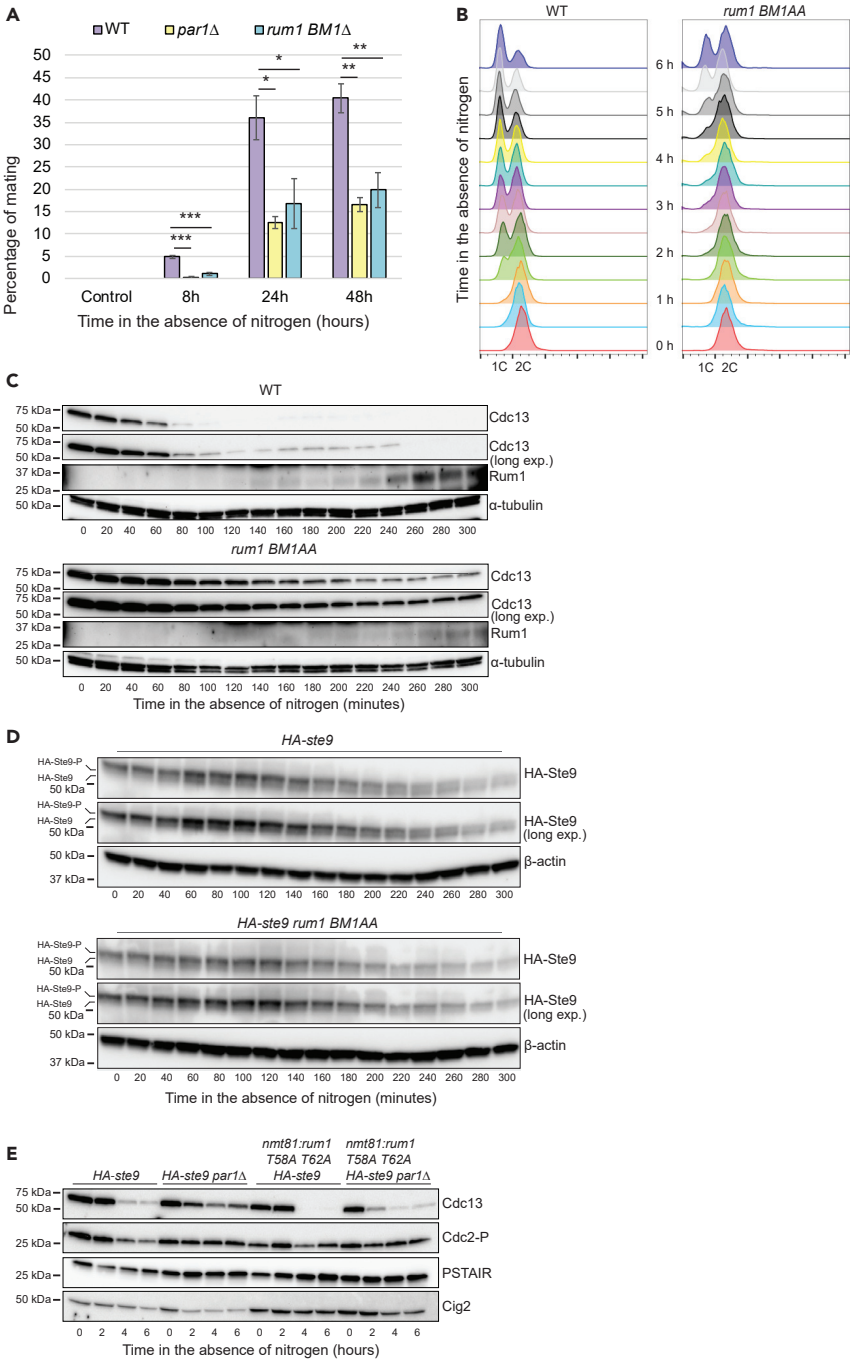

Figure 7. Mutation of a Putative SLiM Motif of PP2A-B56 in Rum1 Phenocopies the Deletion of *par1*

(A) Homothallic WT, *par1*Δ, and *rum1 BM1AA* cells were incubated at 25°C in the absence of nitrogen, and their mating efficiency was determined after 0, 8, 24, and 48 h. Mean values of three biological repeats ± SD is shown. Statistical significance of the difference between strains was assessed with a t test assuming two-tailed distribution and unequal variance. *$p < 0.05$, **$p < 0.01$, and ***$p < 0.001$.

(B) Flow cytometric analysis of the DNA content of WT and *rum1 BM1AA* cells collected every 30 min during a time course of 6 h in the absence of nitrogen.

(C) WT and *rum1 BM1AA* cells were incubated at 25°C in the absence of nitrogen, and samples were collected at the indicated time points. Western blots show protein levels of Cdc13 and Rum1. α-Tubulin was used as loading control.

Figure 7. *Continued*

(D) *HA-ste9* and *HA-ste9 rum1 BM1AA* cells were maintained at 25°C without nitrogen, and samples were collected at the indicated time points. Ste9 was detected by western blot against its N-terminal HA-tag, and β-actin served as loading control. HA, hemagglutinin.

(E) *HA-Ste9*, *HA-Ste9 par1*Δ, *HA-Ste9 nmt81*::*rum1 T58A T62A*, and *HA-Ste9 nmt81*::*rum1 T58A T62A par1*Δ cells were incubated for 24 h in the absence of thiamine for the expression of Rum1 T58A T62A. Cells were washed with four volumes of EMM-N before resuspending them in EMM-N, and samples were collected at the indicated time points. Protein levels of Cdc13 and Cig2, and phosphorylation of Cdc2 Tyr15 were determined by western blot. Total Cdc2 (PSTAIR) was used as loading control.

See also Figure S7.

Fission yeast cells grown in the presence of glucose and a rich nitrogen source have a very short G1 phase and enter S phase shortly after completion of mitosis (so much so that S-phase coincides with cytokinesis). This has been explained as the consequence of cells exiting mitosis having attained the sufficient cell size to satisfy a G1 cell size checkpoint (that under these circumstances is cryptic) (Moreno and Nurse, 1994). From a molecular point of view, this could also be understood as cells exiting mitosis with sufficient CDK activity to progress through Start and initiate DNA replication (Stern and Nurse, 1996; Coudreuse and Nurse, 2010). Indeed, in synchronized mitotic cultures Cig2 (the S-phase cyclin) starts to accumulate as soon as the mitotic cyclin Cdc13 is degraded (Yamano et al., 2000). However, under poor nutritional conditions (a more likely representation of conditions in nature) cell growth is limited and the cell needs to engage molecular brakes that delay or completely halt (in the absence of a nitrogen source) progression through Start. This is mediated by the accumulation of the CKI Rum1 and the activation of the APC/C activator Ste9 that prevent the activation of CDK complexes. Both Rum1 and Ste9 establish double-negative feedback loops with CDK complexes with varying strength depending on the associated cyclin (Benito et al., 1998; Blanco et al., 2000) that render the system bistable (high- versus low-CDK states) and the transitions between these two states irreversible. Here, we have shown that in the absence of PP2A-B56^{Par1} activity, degradation of Cdc13 is impaired, and this results in the failure to properly arrest cell cycle progression in G1. This defect correlates with the inability of *par1*Δ cells to dephosphorylate the APC activator Ste9 or to stabilize the CKI Rum1. Moreover, all these defects can be efficiently rescued through the deletion of the G1/S cyclins Cig1 and Cig2, which supports the idea that PP2A-B56^{Par1} directly controls the dephosphorylation of these CDK inhibitors. This conclusion is also reinforced by the fact that expression of a mutant version of Rum1 lacking a putative B56 SLiM (*rum1 BM1AA*) depicts similar mating and cell cycle defects to the *par1*Δ mutant upon nitrogen depletion. Importantly, our conclusions are not only limited to the nitrogen starvation response. The deletion of *par1* impairs the extension of G1 phase that is required when the growth during G2 is limited (as in a *wee1-50* mutant) or when expression of the genes needed for S-phase is blocked (as in a *cdc10-V50* mutant). All this translates to the fact that when PP2A-B56^{Par1} is not present, the cell is less responsive to the signaling cues indicating that cell cycle progression needs to come to a halt and that CDK activity needs to be kept low.

The budding yeast counterparts of Rum1 and Ste9, Sic1 and Cdh1/Hct1, are dephosphorylated by Cdc14 during mitotic exit (Zachariae, 1998; Visintin et al., 1998; Jaspersen et al., 1999). However, the Cdc14 homolog in fission yeast, Clp1/Flp1, was shown early on not to affect Rum1 and Ste9 phosphorylation status (Cueille et al., 2001). Recent reports indicate that PP2A-B55 is the preferential phosphatase counteracting CDK phosphorylation events, whereas PP2A-B56 is in charge of removing Aurora-dependent (and other mitotic kinases') phosphorylations (Cundell et al., 2016; Godfrey et al., 2017; Saurin, 2018). In the case of Rum1, however, we could not identify a bipartite basic patch mediating the interaction to B55 as described in the study by Cundell et al., whereas two putative B56 binding motifs were present (Hertz et al., 2016). It is worth noting that in fission yeast PP1, PP2A-B55, and PP2A-B56 are sequentially activated upon Cdc13 degradation to bring about mitotic exit (Grallert et al., 2015). As PP2A-B56 is the last in this phosphatase relay, it is not surprising that it is in charge of dephosphorylating a late CDK substrate such as Rum1. Intriguingly, we did not identify any potential B56 binding motif in Ste9, although it was clear that its dephosphorylation was impaired in the *par1*Δ mutant. This could have different explanations: it could be that in this case binding to B56 is mediated through a motif other than the LxxIxE SLiM described by Hertz et al. or through additional proteins. Alternatively, it could be understood as the result of increased CDK activity in the absence of Par1 due to the failure to stabilize Rum1. Several evidences back this hypothesis: first, the complete suppression of the Ste9 dephosphorylation defect in the triple *par1*Δ *cig1*Δ *cig2*Δ mutant and, second, the fact that either the deletion of *rum1* or the mutation of the B56 binding motif impairs the dephosphorylation of Ste9 to a similar extent (Figures S4E and 7D). Nevertheless, *in vitro* dephosphorylation assays will be needed to determine if Ste9 is a direct PP2A-B56 substrate.

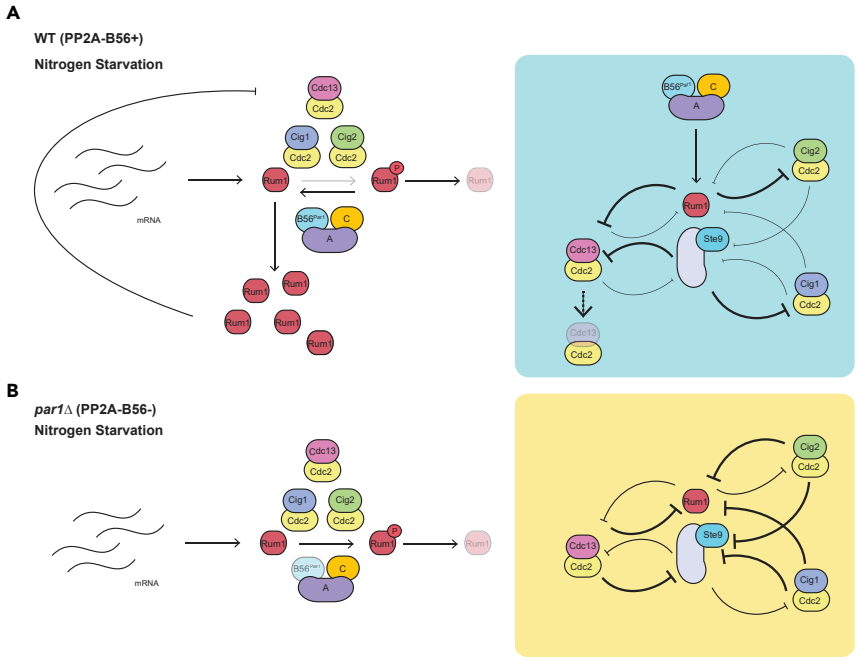

Figure 8. Model

(A) (Left) During the nitrogen starvation response *rum1* mRNA expression is induced and Rum1 protein is produced. CDK complexes phosphorylate and target newly synthesized Rum1 for degradation, but this phosphorylation is opposed by PP2A-B56^{Par1}, which leads to the stabilization of Rum1. As Rum1 accumulates, this eventually results in the sustained inactivation of CDK complexes. (Right) Owing to the presence of double-negative feedback loops between CDK complexes and their inhibitors, inactivation of CDK complexes leads to the further stockpiling of Rum1 and the termination of the inhibition of Ste9.

(B) (Left) In the absence of PP2A-B56 activity, Rum1 phosphorylation mediated by CDK complexes cannot be counteracted and Rum1 does not accumulate in the cell. (Right) In consequence CDK complexes are not inhibited and can repress APC/C-Ste9 activity, resulting in impaired degradation of Cdc13.

In mammalian cells, a great body of evidence has underscored the importance of the CIP/KIP CKIs p21, p27, and p57 during differentiation and quiescence (Coats et al., 1999; Zhang et al., 1997, 1998; 1999; Tury et al., 2011; Gosselet et al., 2007). Coincidentally, B56 subunits were originally shown to be enriched in adult brain and to be induced in neuroblastoma cell lines in response to retinoic acid (McCright et al., 1996). Moreover, PP2A-B56 was one of the signature genes upregulated during the initiation of quiescence induced by contact inhibition in fibroblast cultures (Coller et al., 2006). Of all CIP/KIP members only p57 contains a putative B56 binding motif. Nevertheless, several reports indicate that B56γ can dephosphorylate p27, leaving open the possibility that in this case interaction is mediated by a different motif or through additional proteins. These observations and our results open the possibility that in higher eukaryotes also PP2A-B56 enzymes contribute to the activation of CKIs during cell differentiation and quiescence.

In addition, p21 is an important element controlling the activation of the bistable Rb-E2F switch that dictates passage through the restriction point and that determines the depth of quiescence (Kwon et al., 2017; Moser et al., 2018). p21 sets the threshold of CDK2 activity that governs this transition and the decision to commit to a new round of division or enter a quiescent state (Spencer et al., 2013; Overton et al., 2014). Using a fluorescent sensor of CDK2 activity, Spencer et al. identified two different populations at the end of mitosis: one wherein CDK2 activity started to increase immediately after mitosis from an intermediate level and another population that exited mitosis with low CDK2 activity and that entered a reversible G0 state (Spencer et al., 2013). In the first instance, the level of p21 was low and the decision to commit to a new cell cycle was made at the end of mitosis, much earlier than traditionally believed. Only in cells that exited mitosis with high levels of p21 and low CDK2 activity, mitogenic stimulation was needed to progress through the restriction point. Nevertheless, a later study using fibroblast primary cultures did show that, in this cell type, commitment to a new division was only occurring during G1 phase upon mitogenic stimulation (Schwarz et al., 2018). Although this discrepancy may be due to differences in the experimental setup, it could also indicate that the premature passage through the restriction point is favored in immortalized/cancer-

derived cell lines and not the representation of a normal cell cycle regulation. One of the properties of cancer cells is their ability to divide even in the absence of mitogens. Although this can result from the exacerbated signaling of a wealth of pathways, the incomplete downregulation of CDK activity during mitotic exit can clearly also contribute. We have observed that in mitotically synchronized fission yeast cells lacking PP2A-B56 activity mitotic exit occurs in the presence of residual Cdc13 (Nathalia Chica and Sandra Lopez-Aviles, Unpublished Data). Could loss of B56 activity in cancer cells also alter their responsiveness to environmental signals? Given that PP2A regulatory subunits are frequently mutated in cancer (reviewed in Ruvolo, 2016) this is an idea worth investigating in the future.

Limitations of the Study

This study describes a role for PP2A-B56^{Par1} in mediating the downregulation of CDK activity during G1, which is critical during quiescence and differentiation. In the absence of PP2A-B56^{Par1} activity, the degradation of the mitotic cyclin Cdc13, the dephosphorylation of the APC activator Ste9, and the stabilization of the CDK inhibitor Rum1 are impaired.

However, the low Ste9 and Rum1 protein level has complicated the execution *of in vivo* biochemical assays and we have been limited to assays using purified proteins. In the case of Ste9, whose binding to Par1 *in vitro* was very weak, however clearly affected by the absence of PP2A-B56^{Par1}, we cannot exclude the possibility that it is a direct target, albeit in that case the interaction should be mediated by additional proteins. Still, we lean toward a scenario wherein impaired stabilization of Rum1 in the *par1* mutant background results in increased CDK activity and sustained phosphorylation of Ste9. Similarly, although we have seen that mutation of a putative B56 binding motif in Rum1 phenocopies the defects of the *par1* deletion, we have not been able to show that the mutation affects the interaction with PP2A-B56^{Par1} *in vivo*.

In the future, structural studies and *in vitro* phosphatase assays will provide further insight into the relationship between PP2A-B56^{Par1}, Rum1, and Ste9.

METHODS

All methods can be found in the accompanying Transparent Methods supplemental file.

SUPPLEMENTAL INFORMATION

Supplemental Information can be found online at https://doi.org/10.1016/j.isci.2020.101063.

ACKNOWLEDGMENTS

We thank Sergio Moreno and Jacky Hayles for sharing strains and reagents and for stimulating discussion. We thank Frank Uhlmann, Beata Grallert, Rosa Aligue, Toni Hurtado, and the members of the Lopez-Aviles lab for critical reading of the manuscript. V.S., D.S.-P., N.S., and S.L.-A. are supported by the Centre for Molecular Medicine Norway (NCMM), the Department of Chemistry (N.S.), and the Department of Biosciences (S.L.-A.) at University of Oslo. The research of R.M. is supported by a grant from the Norwegian Research Council awarded to S.L.-A. (FRIMEDBIO 251321). N.S. is supported by a grant from the Norwegian Research Council (FRIMEDBIO 263195).

AUTHOR CONTRIBUTIONS

Conceptualization: S.L.-A. and R.M.; Methodology: V.S., R.M., D.S.-P., N.S., and S.L.-A.; Investigation: V.S., R.M., and D.S.-P.; Resources: N.S. and S.L.-A.; Writing – Original Draft: S.L.-A. and R.M.; Writing – Review and Editing V.S., R.M., D.S.-P., N.S., and S.L.-A.; Visualization: V.S., R.M., and S.L.-A.; Supervision: S.L.-A.; Funding Acquisition: S.L.-A.

DECLARATION OF INTEREST

The authors declare no competing interests.

Received: December 16, 2019
Revised: March 15, 2020
Accepted: April 9, 2020
Published: May 22, 2020

REFERENCES

Barr, A.R., Cooper, S., Heldt, F.S., Butera, F., Stoy, H., Mansfeld, J., Novák, B., and Bakal, C. (2017). DNA damage during S-phase mediates the proliferation-quiescence decision in the subsequent G1 via p21 expression. Nat. Commun. *8*, 14728.

Barr, A.R., Heldt, F.S., Zhang, T., Bakal, C., and Novák, B. (2016). A dynamical framework for the all-or-none G1/S transition. Cell Syst. *2*, 27–37.

Benito, J., Martín-Castellanos, C., and Moreno, S. (1998). Regulation of the G1 phase of the cell cycle by periodic stabilization and degradation of the p25rum1 CDK inhibitor. EMBO J. *17*, 482–497.

Blanco, M.A., Sánchez-Díaz, A., de Prada, J.M., and Moreno, S. (2000). APC(ste9/srw1) promotes degradation of mitotic cyclins in G(1) and is inhibited by cdc2 phosphorylation. EMBO J. *19*, 3945–3955.

Bouchoux, C., and Uhlmann, F. (2011). A quantitative model for ordered cdk substrate dephosphorylation during mitotic exit. Cell *147*, 803–814.

Cheung, T.H., and Rando, T.A. (2013). Molecular regulation of stem cell quiescence. Nat. Rev. Mol. Cell Biol. *14*, 329–340.

Coats, S., Whyte, P., Fero, M.L., Lacy, S., Chung, G., Randel, E., Firpo, E., and Roberts, J.M. (1999). A new pathway for mitogen-dependent cdk2 regulation uncovered in p27(Kip1)-deficient cells. Curr. Biol. *9*, 163–173.

Coller, H.A., Sang, L., and Roberts, J.M. (2006). A new description of cellular quiescence. PLoS Biol. *4*, e83.

Correa-Bordes, J. (1997). p25rum1 promotes proteolysis of the mitotic B-cyclin p56cdc13 during G1 of the fission yeast cell cycle. EMBO J. *16*, 4657–4664.

Correa-Bordes, J., and Nurse, P. (1995). p25rum1 orders S phase and mitosis by acting as an inhibitor of the p34cdc2 mitotic kinase. Cell *83*, 1001–1009.

Coudreuse, D., and Nurse, P. (2010). Driving the cell cycle with a minimal CDK control network. Nature *468*, 1074–1079.

Cueille, N., Salimova, E., Esteban, V., Blanco, M., Moreno, S., Bueno, A., and Simanis, V. (2001). Flp1, a fission yeast orthologue of the s. cerevisiae CDC14 gene, is not required for cyclin degradation or rum1p stabilisation at the end of mitosis. J. Cell Sci. *114*, 2649–2664.

Cundell, M.J., Hutter, L.H., Nunes Bastos, R., Poser, E., Holder, J., Mohammed, S., Novák, B., and Barr, F.A. (2016). A PP2A-B55 recognition signal controls substrate dephosphorylation kinetics during mitotic exit. J. Cell Biol. *214*, 539–554.

Dalton, S. (2015). Linking the cell cycle to cell fate decisions. TrendsCell Biol. *25*, 592–600.

Deng, C., Zhang, P., Wade Harper, J., Elledge, S.J., and Leder, P. (1995). Mice Lacking p21CIP1/WAF1 undergo normal development, but are defective in G1 checkpoint control. Cell *82*, 675–684.

Dulić, V., Kaufmann, W.K., Wilson, S.J., Tlsty, T.D., Lees, E., Harper, J.W., Elledge, S.J., and Reed, S.I. (1994). p53-dependent inhibition of cyclin-dependent kinase activities in human fibroblasts during radiation-induced G1 arrest. Cell *76*, 1013–1023.

Enoch, T., and Nurse, P. (1990). Mutation of fission yeast cell cycle control genes abolishes dependence of mitosis on DNA replication. Cell *60*, 665–673.

Fantes, P.A. (1981). Isolation of cell size mutants of a fission yeast by a new selective method: characterization of mutants and implications for division control mechanisms. J. Bacteriol. *146*, 746.

Fiore, A.P.Z.P., Ribeiro, P.de F., and Bruni-Cardoso, A. (2018). Sleeping beauty and the microenvironment enchantment: microenvironmental regulation of the proliferation-quiescence decision in normal tissues and in cancer development. Front. Cell Dev. Biol. *6*, 59.

Fisher, D., and Nurse, P. (1995). Cyclins of the fission yeast Schizosaccharomyces pombe. Semin. Cell Biol. *6*, 73–78.

Fisher, D.L., and Nurse, P. (1996). A single fission yeast mitotic cyclin B p34cdc2 kinase promotes both S-phase and mitosis in the absence of G1 cyclins. EMBO J. *15*, 850–860.

Gharbi-Ayachi, A., Labbé, J.-C., Burgess, A., Vigneron, S., Strub, J.-M., Brioudes, E., Van-Dorsselaer, A., Castro, A., and Lorca, T. (2010). The substrate of Greatwall kinase, Arpp19, controls mitosis by inhibiting protein phosphatase 2A. Science *330*, 1673–1677.

Godfrey, M., Touati, S.A., Kataria, M., Jones, A., Snijders, A.P., and Uhlmann, F. (2017). PP2A(Cdc55) phosphatase imposes ordered cell-cycle phosphorylation by opposing threonine phosphorylation. Mol. Cell *65*, 393–402.e3.

Gosselet, F.P., Magnaldo, T., Culerrier, R.M., Sarasin, A., and Ehrhart, J.-C. (2007). BMP2 and BMP6 control p57(Kip2) expression and cell growth arrest/terminal differentiation in normal primary human epidermal keratinocytes. Cell Signal. *19*, 731–739.

Gould, K.L., and Nurse, P. (1989). Tyrosine phosphorylation of the fission yeast cdc2+ protein kinase regulates entry into mitosis. Nature *342*, 39–45.

Gouw, M., Michael, S., Sámano-Sánchez, H., Kumar, M., Zeke, A., Lang, B., Bely, B., Chemes, L.B., Davey, N.E., Deng, Z., et al. (2018). The eukaryotic linear motif resource - 2018 update. Nucleic Acids Res. *46*, D428–D434.

Grallert, A., Boke, E., Hagting, A., Hodgson, B., Connolly, Y., Griffiths, J.R., Smith, D.L., Pines, J., and Hagan, I.M. (2015). A PP1-PP2A phosphatase relay controls mitotic progression. Nature *517*, 94–U248.

Hayward, D., Alfonso Pérez, T., and Gruneberg, U. (2019). Orchestration of the spindle assembly checkpoint by CDK1-cyclin B1. FEBS Lett. *246*, 629–719.

Heldt, F.S., Barr, A.R., Cooper, S., Bakal, C., and Novák, B. (2018). A comprehensive model for the proliferation–quiescence decision in response to endogenous DNA damage in human cells. Proc. Natl. Acad. Sci. U S A *115*, 2532.

Hertz, E.P.T., Kruse, T., Davey, N.E., López-Méndez, B., Sigurðsson, J.O., Montoya, G., Olsen, J.V., and Nilsson, J. (2016). A conserved motif provides binding specificity to the PP2A-B56 phosphatase. Mol. Cell *63*, 686–695.

Janssens, V., Longin, S., and Goris, J. (2008). PP2A holoenzyme assembly: in cauda venenum (the sting is in the tail). Trends Biochem. Sci. *33*, 113–121.

Jaspersen, S.L., Charles, J.F., and Morgan, D.O. (1999). Inhibitory phosphorylation of the APC regulator Hct1 is controlled by the kinase Cdc28 and the phosphatase Cdc14. Curr. Biol. *9*, 227–236.

Jiang, W., and Hallberg, R.L. (2000). Isolation and characterization of par1(+) and par2(+): two Schizosaccharomyces pombe genes encoding B′ subunits of protein phosphatase 2A. Genetics *154*, 1025–1038.

Kitamura, K., Maekawa, H., and Shimoda, C. (1998). Fission yeast Ste9, a homolog of Hct1/Cdh1 and Fizzy-related, is a novel negative regulator of cell cycle progression during G1-phase. Mol. Biol. Cell *9*, 1065–1080.

Kjaerulff, S., Andersen, N.R., Borup, M.T., and Nielsen, O. (2007). Cdk phosphorylation of the Ste11 transcription factor constrains differentiation-specific transcription to G1. Genes Dev. *21*, 347–359.

Kominami, K., Ochotorena, I., and Toda, T. (1998a). Two F-box/WD-repeat proteins Pop1 and Pop2 form hetero- and homo-complexes together with cullin-1 in the fission yeast SCF (Skp1-Cullin-1-F-box) ubiquitin ligase. Genes Cells *3*, 721–735.

Kominami, K., Seth-Smith, H., and Toda, T. (1998b). Apc10 and Ste9/Srw1, two regulators of the APC-cyclosome, as well as the CDK inhibitor Rum1 are required for G1 cell-cycle arrest in fission yeast. EMBO J. *17*, 5388–5399.

Kominami, K., and Toda, T. (1997). Fission yeast WD-repeat protein pop1 regulates genome ploidy through ubiquitin-proteasome-mediated degradation of the CDK inhibitor Rum1 and the S-phase initiator Cdc18. Genes Dev. *11*, 1548–1560.

Kruse, T., Biedenkopf, N., Hertz, E.P.T., Dietzel, E., Stalmann, G., López-Méndez, B., Davey, N.E., Nilsson, J., and Becker, S. (2018). The ebola virus nucleoprotein recruits the host PP2A-B56 phosphatase to activate transcriptional support activity of VP30. Mol. Cell *69*, 136–145.e6.

Kwon, J.S., Everetts, N.J., Wang, X., Wang, W., Della Croce, K., Xing, J., and Yao, G. (2017). Controlling depth of cellular quiescence by an Rb-E2F network switch. Cell Rep. *20*, 3223–3235.

Lopez-Aviles, S., Grande, M., González, M., Helgesen, A.-L., Alemany, V., Sanchez-Piris, M., Bachs, O., Millar, J.B.A., and Aligue, R. (2005). Inactivation of the Cdc25 phosphatase by the

stress-activated Srk1 kinase in fission yeast. Mol. Cell *17*, 49–59.

Manchado, E., Guillamot, M., de Cárcer, G., Eguren, M., Trickey, M., García-Higuera, I., Moreno, S., Yamano, H., Cañamero, M., and Malumbres, M. (2010). Targeting mitotic exit leads to tumor regression in vivo: modulation by Cdk1, mastl, and the PP2A/B55α,δ phosphatase. Cancer Cell *18*, 641–654.

Martín, R., Portantier, M., Chica, N., Nyquist-Andersen, M., Mata, J., and Lopez-Aviles, S. (2017). A PP2A-B55-mediated crosstalk between TORC1 and TORC2 regulates the differentiation response in fission yeast. Curr. Biol. *27*, 175–188.

Martín-Castellanos, C., Labib, K., and Moreno, S. (1996). B-type cyclins regulate G1 progression in fission yeast in opposition to the p25rum1 cdk inhibitor. EMBO J. *15*, 839–849.

Matsumoto, A., Takeishi, S., Kanie, T., Susaki, E., Onoyama, I., Tateishi, Y., Nakayama, K., and Nakayama, K.I. (2011). p57 is required for quiescence and maintenance of adult hematopoietic stem cells. Cell Stem Cell *9*, 262–271.

Mayer-Jaekel, R.E., Ohkura, H., Ferrigno, P., Andjelkovic, N., Shiomi, K., Uemura, T., Glover, D.M., and Hemmings, B.A. (1994). Drosophila mutants in the 55 kDa regulatory subunit of protein phosphatase 2A show strongly reduced ability to dephosphorylate substrates of p34cdc2. J. Cell Sci. *107* (Pt 9), 2609–2616.

McCright, B., Rivers, A.M., Audlin, S., and Virshup, D.M. (1996). The B56 family of protein phosphatase 2A (PP2A) regulatory subunits encodes differentiation-induced phosphoproteins that target PP2A to both nucleus and cytoplasm. J. Biol. Chem. *271*, 22081–22089.

Mochida, S., Ikeo, S., Gannon, J., and Hunt, T. (2009). Regulated activity of PP2A–B55δ is crucial for controlling entry into and exit from mitosis in Xenopus egg extracts. EMBO J. *28*, 2777–2785.

Mochida, S., Maslen, S.L., Skehel, M., and Hunt, T. (2010). Greatwall phosphorylates an inhibitor of protein phosphatase 2A that is essential for mitosis. Science *330*, 1670–1673.

Mondesert, O., McGowan, C.H., and Russell, P. (1996). Cig2, a B-type cyclin, promotes the onset of S in Schizosaccharomyces pombe. Mol. Cell Biol. *16*, 1527–1533.

Moreno, S., and Nurse, P. (1994). Regulation of progression through the G1 phase of the cell cycle by the rum1+ gene. Nature *367*, 236–242.

Moser, J., Miller, I., Carter, D., and Spencer, S.L. (2018). Control of the restriction point by Rb and p21. Proc. Natl. Acad. Sci. U S A *115*, E8219.

Novak, B., Csikasz-Nagy, A., Gyorffy, B., Chen, K., and Tyson, J.J. (1998). Mathematical model of the fission yeast cell cycle with checkpoint controls at the G1/S, G2/M and metaphase/anaphase transitions. Biophys. Chem. *72*, 185–200.

Oesterle, E.C., Chien, W.-M., Campbell, S., Nellimarla, P., and Fero, M.L. (2011). p27Kip1 is required to maintain proliferative quiescence in the adult cochlea and pituitary. Cell Cycle *10*, 1237–1248.

O'Farrell, P.H. (2011). Quiescence: early evolutionary origins and universality do not imply uniformity. Philos. Trans. R. Soc. B Biol. Sci. *366*, 3498–3507.

Overton, K.W., Spencer, S.L., Noderer, W.L., Meyer, T., and Wang, C.L. (2014). Basal p21 controls population heterogeneity in cycling and quiescent cell cycle states. Proc. Natl. Acad. Sci. U S A *111*, E4386.

Parker, L.L., Atherton-Fessler, S., and Piwnica-Worms, H. (1992). p107wee1 is a dual-specificity kinase that phosphorylates p34cdc2 on tyrosine 15. Proc. Natl. Acad. Sci. U S A *89*, 2917–2921.

Russell, P., and Nurse, P. (1987). Negative regulation of mitosis by wee1+, a gene encoding a protein kinase homolog. Cell *49*, 559–567.

Ruvolo, P.P. (2016). The broken 'Off' switch in cancer signaling: PP2A as a regulator of tumorigenesis, drug resistance, and immune surveillance. BBA Clin. *6*, 87–99.

Saurin, A.T. (2018). Kinase and phosphatase cross-talk at the kinetochore. Front. Cell Dev. Biol. *6*, 2964–3023.

Schmitz, M.H.A., Held, M., Janssens, V., Hutchins, J.R.A., Hudecz, O., Ivanova, E., Goris, J., Trinkle-Mulcahy, L., Lamond, A.I., Poser, I., et al. (2010). Live-cell imaging RNAi screen identifies PP2A–B55α and importin-β1 as key mitotic exit regulators in human cells. Nat. Cell Biol. *12*, 886–893.

Schwarz, C., Johnson, A., Kõivomägi, M., Zatulovskiy, E., Kravitz, C.J., Doncic, A., and Skotheim, J.M. (2018). A precise cdk activity threshold determines passage through the restriction point. Mol. Cell *69*, 253–264.e5.

Spencer, S.L., Cappell, S.D., Tsai, F.-C., Overton, K.W., Wang, C.L., and Meyer, T. (2013). The proliferation-quiescence decision is controlled by a bifurcation in CDK2 activity at mitotic exit. Cell *155*, 369–383.

Stegmeier, F., and Amon, A. (2004). Closing mitosis: the functions of the Cdc14 phosphatase and its regulation. Annu. Rev. Genet. *38*, 203–232.

Stern, B., and Nurse, P. (1996). A quantitative model for the cdc2 control of S phase and mitosis in fission yeast. Trends Genet. *12*, 345–350.

Stern, B., and Nurse, P. (1998). Cyclin B proteolysis and the cyclin-dependent kinase inhibitor rum1p are required for pheromone-induced G 1Arrest in fission yeast. Mol. Biol. Cell *9*, 1309–1321.

Tury, A., Mairet-Coello, G., and DiCicco-Bloom, E. (2011). The cyclin-dependent kinase inhibitor p57Kip2 regulates cell cycle exit, differentiation, and migration of embryonic cerebral cortical precursors. Cereb. Cortex *21*, 1840–1856.

Visintin, R., Craig, K., Hwang, E.S., Prinz, S., Tyers, M., and Amon, A. (1998). The phosphatase Cdc14 triggers mitotic exit by reversal of Cdk-dependent phosphorylation. Mol. Cell *2*, 709–718.

Wang, X., Bajaj, R., Bollen, M., Peti, W., and Page, R. (2016). Expanding the PP2A interactome by defining a B56-specific SLiM. Structure *24*, 2174–2181.

Wu, J.Q., Guo, J.Y., Tang, W., Yang, C.-S., Freel, C.D., Chen, C., Nairn, A.C., and Kornbluth, S. (2009). PP1-mediated dephosphorylation of phosphoproteins at mitotic exit is controlled by inhibitor-1 and PP1 phosphorylation. Nat. Cell Biol. *11*, 644–651.

Wu, L., and Russell, P. (1997). Roles of Wee1 and Nim1 protein kinases in regulating the switch from mitotic division to sexual development in Schizosaccharomyces pombe. Mol. Cell Biol. *17*, 10–17.

Yamaguchi, S., Murakami, H., and Okayama, H. (1997). A WD repeat protein controls the cell cycle and differentiation by negatively regulating Cdc2/B-type cyclin complexes. Mol. Biol. Cell *8*, 2475–2486.

Yamano, H., Kitamura, K., Kominami, K., Lehmann, A., Katayama, S., Hunt, T., and Toda, T. (2000). The spike of S phase cyclin Cig2 expression at the G1-S border in fission yeast requires both APC and SCF ubiquitin ligases. Mol. Cell *6*, 1377–1387.

Zachariae, W. (1998). Control of cyclin ubiquitination by CDK-regulated binding of Hct1 to the anaphase promoting complex. Science *282*, 1721–1724.

Zarzov, P., Decottignies, A., Baldacci, G., and Nurse, P. (2002). G(1)/S CDK is inhibited to restrain mitotic onset when DNA replication is blocked in fission yeast. EMBO J. *21*, 3370–3376.

Zeng, Y., Forbes, K.C., Wu, Z., Moreno, S., Piwnica-Worms, H., and Enoch, T. (1998). Replication checkpoint requires phosphorylation of the phosphatase Cdc25 by Cds1 or Chk1. Nature *395*, 507–510.

Zhang, P., Liégeois, N.J., Wong, C., Finegold, M., Hou, H., Thompson, J.C., Silverman, A., Harper, J.W., DePinho, R.A., and Elledge, S.J. (1997). Altered cell differentiation and proliferation in mice lacking p57KIP2 indicates a role in Beckwith-Wiedemann syndrome. Nature *387*, 151–158.

Zhang, P., Wong, C., DePinho, R.A., Harper, J.W., and Elledge, S.J. (1998). Cooperation between the Cdk inhibitors p27(KIP1) and p57(KIP2) in the control of tissue growth and development. Genes Dev. *12*, 3162–3167.

Zhang, P., Wong, C., Liu, D., Finegold, M., Harper, J.W., and Elledge, S.J. (1999). p21(CIP1) and p57(KIP2) control muscle differentiation at the myogenin step. Genes Dev. *13*, 213–224.

iScience, Volume *23*

Supplemental Information

Requirement of PP2A-B56^{Par1} for the Stabilization of the CDK Inhibitor Rum1 and Activation of APC/C^{Ste9} during Pre-Start G1 in *S. pombe*

Vilte Stonyte, Ruth Martín, Dario Segura-Peña, Nikolina Sekulić, and Sandra Lopez-Aviles

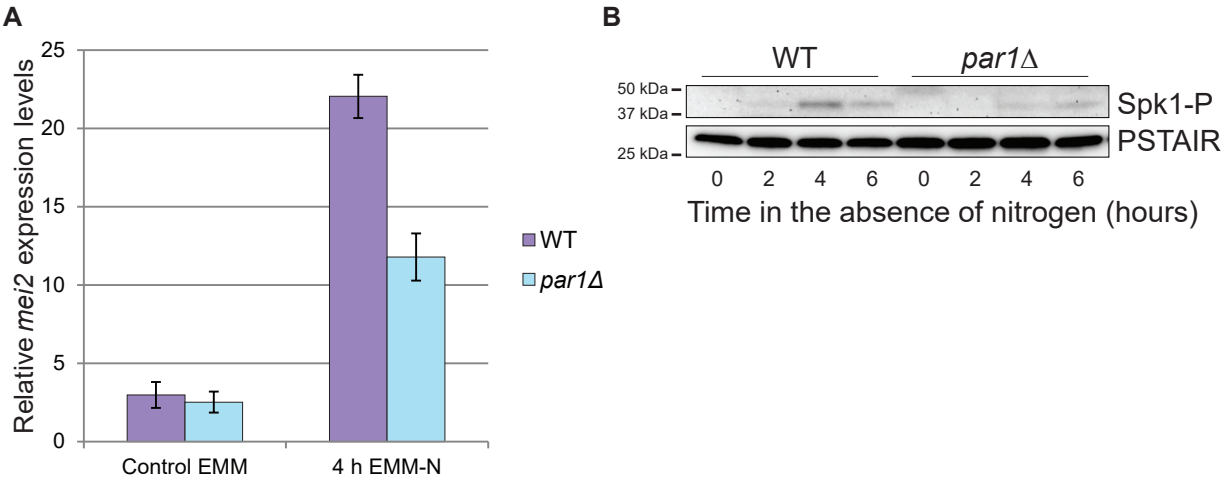

Figure S1. PP2A-B56 activity is required for an adequate expression of *mei2*. Related to Figure 1.

A, mRNA expression of *mei2* in homothallic WT and *par1*Δ cells that had been incubated in EMM (control) or EMM-N for 4 h. Gene expression was determined by qPCR and normalized to *act1* expression. Mean and SEM of four biological replicates are shown. **B**, phosphorylation of the mating pheromone responsive MAPK Spk1 was used as a measure of the pheromone signaling in homothallic WT and *par1*Δ cells deprived of nitrogen. Total Cdc2 (PSTAIR) served as loading control.

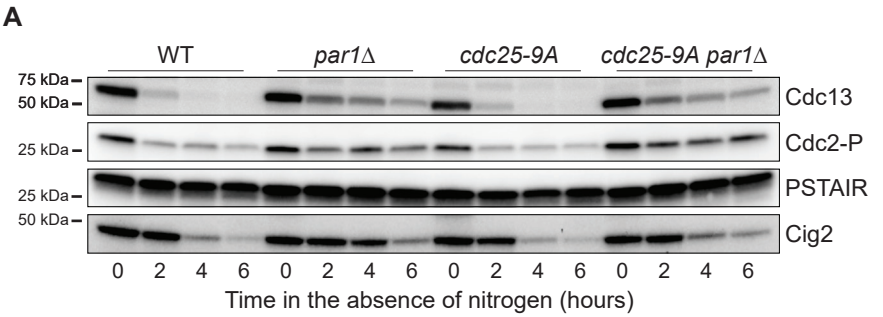

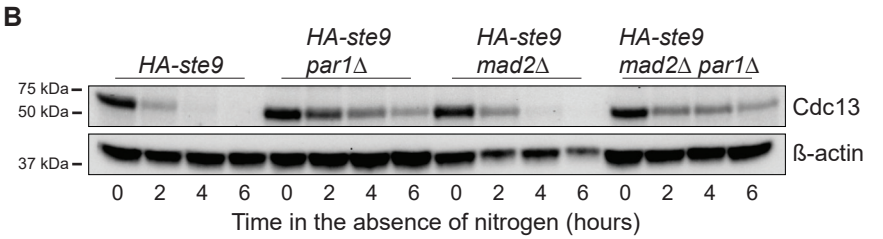

Figure S2. Accelerating mitotic entry or overriding the SAC does not rescue the Cdc13 degradation defect of a par1Δ mutant. Related to Figure 2.

A, heterothallic h- WT, *par1*Δ, *cdc25-9A* and *cdc25-9A par1*Δ cells were incubated at 25 °C in the absence of nitrogen and samples were collected at the indicated time points. Western blots show protein levels of Cdc13 and Cig2, phosphorylation of Cdc2 on Tyr15 and total Cdc2 (PSTAIR) as loading control. **B**, homothallic *HA-ste9*, *HA-ste9 par1Δ*, *HA-ste9 mad2*Δ and *HA-ste9 mad2*Δ *par1*Δ cells were incubated at 25 °C in the absence of nitrogen and samples were collected at the indicated time points. Protein levels of Cdc13 were followed over the time course by western blot. β-actin was used as loading control.

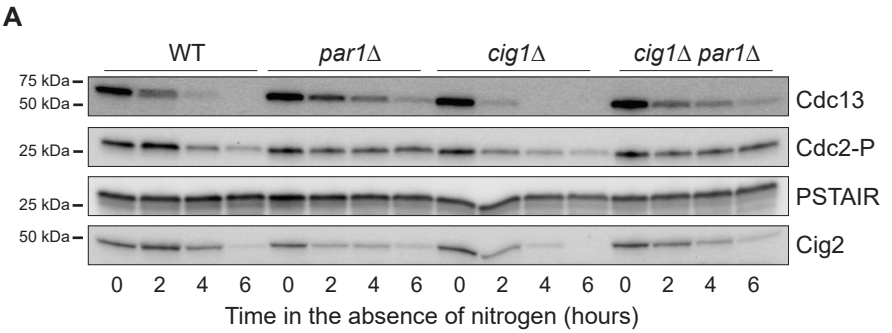

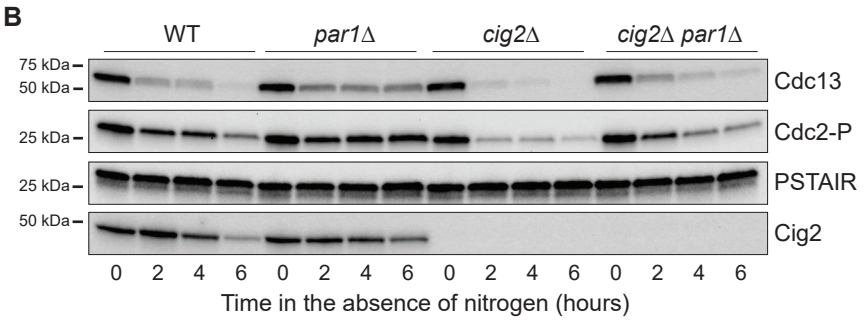

Figure S3. Contribution of the individual deletions of G1/S cyclins to the rescue of the *par1*Δ mutant defect in degradation of Cdc13. Related to Figure 3.

A, homothallic WT, *par1*Δ, *cig1*Δ and *cig1*Δ *par1*Δ cells were incubated at 25 °C in the absence of nitrogen and samples were collected at the indicated time points. Protein levels of Cdc13, Cig2, and phosphorylation of Cdc2 were followed over the time course by western blot. Total Cdc2 (PSTAIR) served as loading control. **B**, homothallic WT, *par1*Δ, *cig2*Δ and *cig2*Δ *par1*Δ cells were incubated at 25 °C in the absence of nitrogen and samples were collected at the indicated time points. Protein levels of Cdc13 and Cig2, and phosphorylation of Cdc2 on Tyr15 were determined by western blot. Total Cdc2 (PSTAIR) was used as loading control.

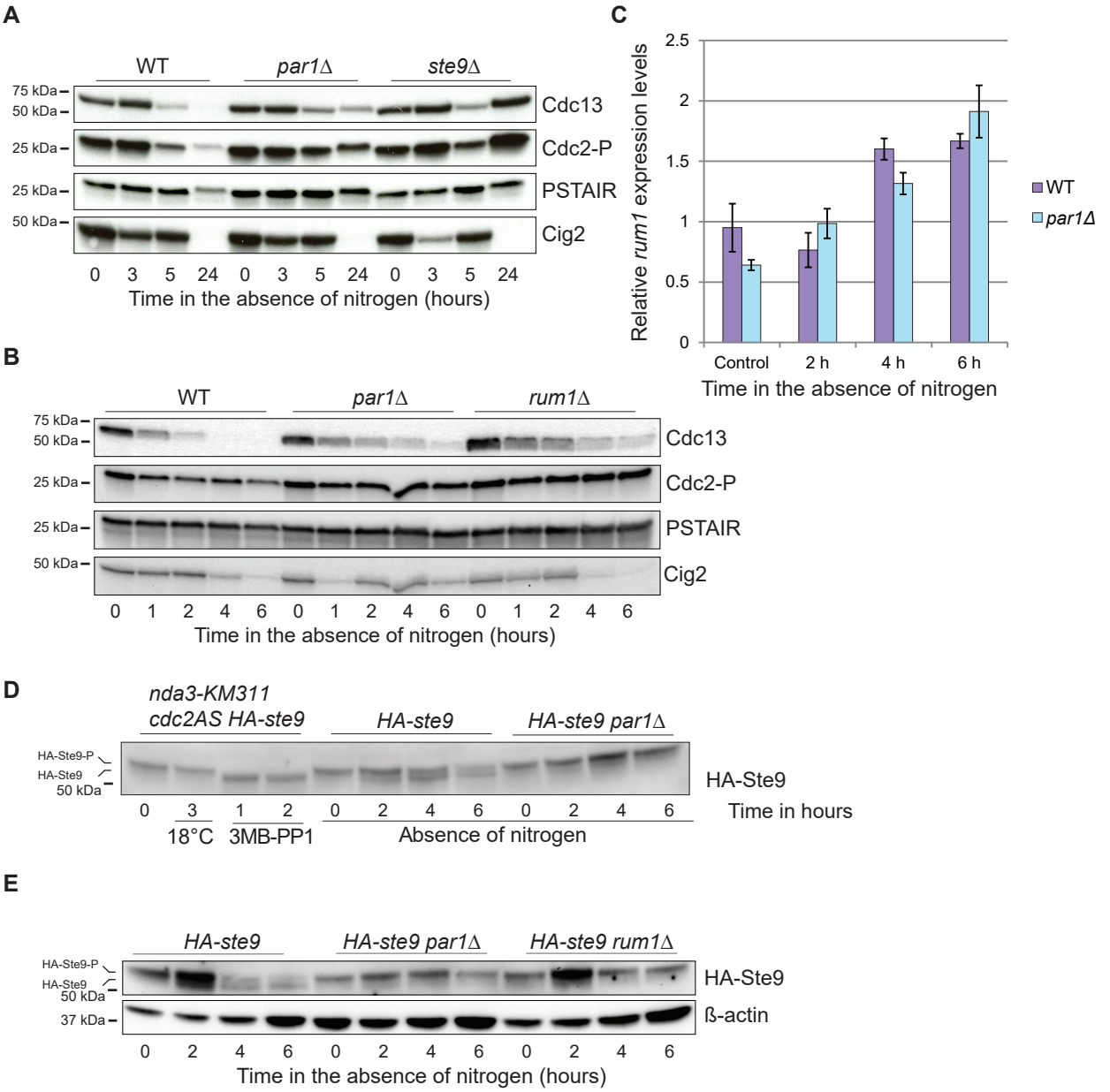

Figure S4. Deletion of *rum1* or *ste9* phenocopies the defects of the *par1*Δ mutant. Related to Figure 4.

A, heterothallic h- WT, *par1*Δ, and *ste9*Δ cells were incubated at 25 °C in the absence of nitrogen and samples were collected at the indicated time points. Western blots show protein levels of Cdc13 and Cig2, and phosphorylation of Cdc2 on Tyr15. Total Cdc2 (PSTAIR) served as loading control. **B**, heterothallic h- WT, *par1*Δ and *rum1*Δ cells were incubated at 25 °C in the absence of nitrogen and samples were collected at the indicated time points. Protein levels of Cdc13 and Cig2, and phosphorylation of Cdc2 on Tyr15 were assessed by western blot. Total Cdc2 (PSTAIR) served as loading control. **C**, mRNA expression of *rum1* in homothallic WT and *par1*Δ cells incubated at 25 °C in EMM (control) for 4 h or in EMM-N for 2, 4 or 6 h. Gene expression was determined by qPCR and normalized to *act1* expression. Mean and SEM of four biological replicates are shown. **D**, *nda3-KM311 cdc2-as HA-ste9* cells were incubated at 18 °C during 3 hours, for a metaphase arrest, or in the presence of 10 μM 3MB-PP1 during 1 and 2 hours, to inhibit Cdc2 activity. *HA-Ste9* and *HA-Ste9 par1*Δ were incubated in the absence of nitrogen at 25 °C and collected at the time points indicated in the figure. Ste9 mobility is shown in a western blot against its N-terminal HA-tag. **E**, homothallic *HA-ste9*, *HA-ste9 par1*Δ and *HA-ste9 rum1*Δ cells were incubated at 25 °C in the absence of nitrogen and samples were collected at the indicated time points. Ste9 was detected by western blot against its N-terminal HA-tag and β-actin as loading control.

Figure S5. Sequences of Par1 inhibitor and mock-inhibitor peptides. Related to Figure 5.
Amino acid sequence of GFP in green, of Par1-inhibitor peptide in yellow and of the mock-inhibitor in purple.

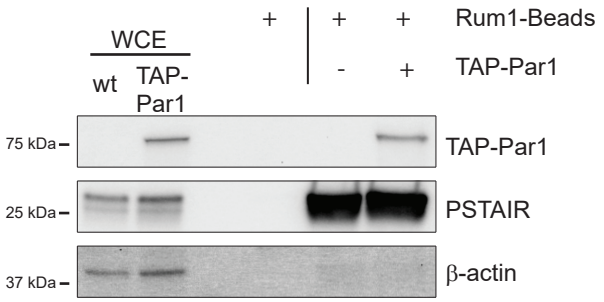

Figure S6. PP2A-B56Par1 co-immunoprecipitates with the CDK inhibitor Rum1 immobilized on beads. Related to Figure 6.

10 mg of total protein from extracts of cells containing TAP-Par1 were incubated with Rum1-coupled magnetic beads. After washing, the bound TAP-Par1 was detected by western blot. Whole cell extract from an untagged WT strain was equally incubated with Rum1-coupled beads and used as a negative control. Western blot shows the interacting TAP-Par1, β-actin as a negative control and Cdc2 (PSTAIR) as a positive control for the binding to Rum1.

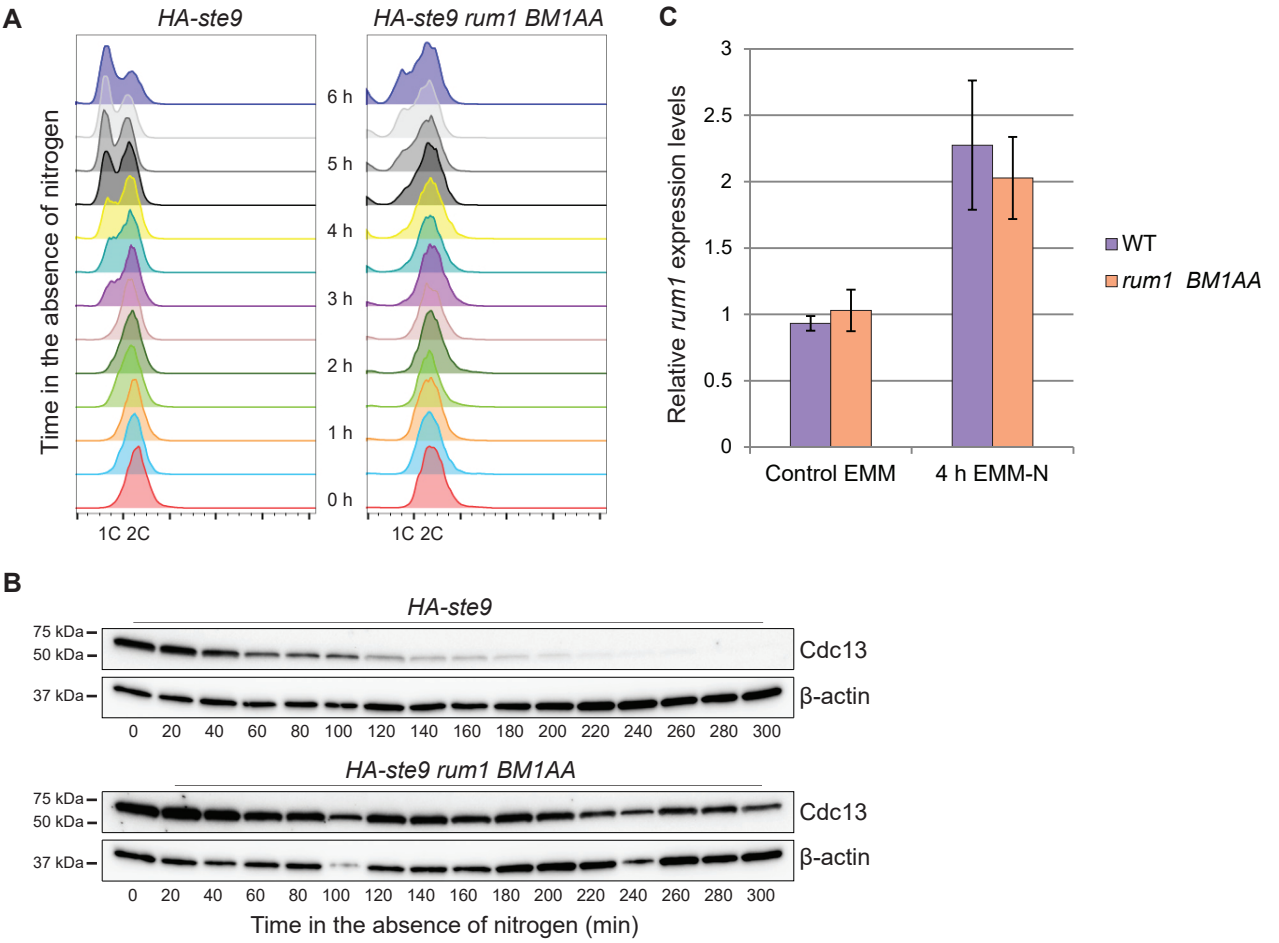

Figure S7. Mutation of a putative SLiM motif of PP2A-B56 in Rum1 phenocopies the deletion of *par1*. Related to Figure 7.

A, flow cytometry analysis of the DNA content of isolated nuclei of heterothallic h- *HA-ste9* and *HA-ste9 rum1 BM1AA* cells collected every 30 minutes during a time course of 6 hours in the absence of nitrogen. **B**, heterothallic h- *HA-ste9* and *HA-ste9 rum1 BM1AA* cells were incubated at 25 °C in the absence of nitrogen and samples were collected at the indicated time points. Western blots show protein levels of Cdc13 and β-actin as loading control.**C**, mRNA expression of *rum1* in homothallic WT and *rum1 BM1AA* cells incubated at 25 °C in EMM (control) or in EMM-N for 4 h. Gene expression was determined by qPCR and normalized to *act1* expression. Mean and SEM of six biological replicates are shown.

Table S1: strains used in this study. Related to Figures 1 to 7 and Figures S1 to S7.

Figure 1		
167	*h90 wt*	Lab stock
343	*h90 Δpab1::kanMX6*	Lab stock
363	*h90 Δpar1::kanMX6*	Lab stock
696	*h90 Δdis2::ura4*	Lab stock
695	*h90 Δclp1::hphMX6*	Lab stock
148	*h- wt*	Lab stock
459	*h- Δpar1::kanMX6*	Lab stock
Figure 2		
148	*h- wt*	Lab stock
459	*h- Δpar1::kanMX6*	Lab stock
594	*h- ade6::ade6+-Padh15-skp1-AtTIR1-2NLS-natMX6- Padh15-skp1-OsTIR1*	Lab stock
796	*h- kanMX6::P41nmt1::3PK-miniAID-par1 ade6::ade6+-Padh15-skp1-AtTIR1-2NLS-natMX6-Padh15-skp1-OsTIR1 Δpar2::kanMX6*	Lab stock
1173	*h- cdc2-3w*	Modified from Rosa Aligue
1672	*h- cdc2-3w Δpar1::kanMX6*	This study
489	*h90 cdc10-V50*	Lab stock
490	*h90 cdc10-V50 Δpar1::kanMX6*	This study
Figure 3		
167	*h90 wt*	Lab stock
363	*h90 Δpar1::kanMX6*	Lab stock
1122	*h90 Δcig1::hphMX6 Δcig2::kanMX6*	This study
1109	*h90 Δcig1::hphMX6 Δcig2::kanMX6 Δpar1::kanMX6*	This study
Figure 4		
1150	*h90 3HA:ste9*	Modified from Sergio Moreno
1148	*h90 3HA:ste9 Δpar1::kanMX6*	This study
1432	*h90 3HA:ste9 Δcig1::hph MX6 Δcig2::kanMX6*	This study
1466	*h90 3HA:ste9 Δcig1::hph MX6 Δcig2::kanMX6 Δpar1::kanMX6*	This study
167	*h90 wt*	Lab stock
363	*h90 Δpar1::kanMX6*	Lab stock
1122	*h90 Δcig1::hphMX6 Δcig2::kanMX6*	This study
1109	*h90 Δcig1::hphMX6 Δcig2::kanMX6 Δpar1::kanMX6*	This study
825	*h90 wee1-50*	Paul Nurse
1146	*h90 wee1-50 Δpar1::kanMX6*	This study
Figure 5		
709	*h+ ura4-294::prom par1-TAP-par1::ura4 Δpar1::kanMX6*	Lab stock
1541	*h- ura4-294::prom par1-TAP-par1::ura4 Δpar1::kanMX6 leu1-32 pREP1-GFP-par1_inh*	This study
1667	*h- ura4-294::prom par1-TAP-par1::ura4 Δpar1::kanMX6 leu1-32 pREP1-GFP-par1_NOinh*	This study
148	*h- wt*	Lab stock
459	*h- Δpar1::kanMX6*	Lab stock
1655	*h- leu1-32 pREP1-GFP-par1_NOinh*	This study
1401	*h- leu1-32 pREP1-GFP-par1_inh*	This study
Figure 6		
709	*h+ ura4-294::prom par1-TAP-par1::ura4 Δpar1::kanMX6*	Lab stock
148	*h- wt*	Lab stock
677	*h+ ura4-294::prom par1-TAP-par1::ura4 Δpar1::kanMX6 leu1-32*	Lab stock
1891	*h- ura4-294::prom par1-TAP-par1F314Q::ura4 Δpar1::kanMX6 leu1-32*	This study
Figure 7		
167	*h90 wt*	Lab stock
363	*h90 Δpar1::kanMX6*	Lab stock
1762	*h90 rum1BM1AA*	This study

1150	*h90 3HA:ste9*	Modified from Sergio Moreno
1749	*h90 3HA:ste9 rum1BM1AA*	This study
148	*h- wt*	Lab stock
1747	*h- rum1BM1AA*	This study
1806	*h- 3HA:ste9*	Modified from Sergio Moreno
1748	*h- 3HA:ste9 rum1BM1AA*	This study
1148	*h90 3HA:ste9 Δpar1::kanMX6*	This study
1777	*h90 3HA:ste9 leu- pJK148 nmt81x rum1 A58 A62*	This study
1771	*h90 3HA:ste9 Δpar1::kanMX6 leu- pJK148 nmt81x rum1 A58 A62*	This study
Figure S1		
167	*h90 wt*	Lab stock
363	*h90 Δpar1::kanMX6*	Lab stock
Figure S2		
148	*h- wt*	Lab stock
459	*h- Δpar1::kanMX6*	Lab stock
1173	*h- cdc25-9A*	Modified from Pedro San-Segundo
1672	*h- cdc25-9A Δpar1::kanMX6*	This study
1150	*h90 3HA:ste9*	Modified from Sergio Moreno
1148	*h90 3HA:ste9 Δpar1::kanMX6*	This study
1339	*h90 3HA:ste9 Δmad2::natMX6*	This study
1380	*h90 3HA:ste9 Δpar1::kanMX6 mad2::natMX6*	This study
Figure S3		
167	*h90 wt*	Lab stock
363	*h90 Δpar1::kanMX6*	Lab stock
1108	*h90 Δcig1::hphMX6*	This study
1117	*h90 Δcig1::hphMX6 Δpar1::kanMX6*	This study
1119	*h90 Δcig2::kanMX6*	This study
1120	*h90 Δcig2::kanMX6 Δpar1::kanMX6*	This study
Figure S4		
148	*h- wt*	Lab stock
459	*h- Δpar1::kanMX6*	Lab stock
1032	*h- Δste9::hphMX6*	This study
968	*rum1::ura4+ ura4D18*	Lab stock
1150	*h90 3HA:ste9*	Modified from Sergio Moreno
1148	*h90 3HA:ste9 Δpar1::kanMX6*	This study
1301	*h90 3HA:ste9 Δrum1::hphMX6*	This study
1207	*h- ste9::5' - 3HA-Ste9 cdc2asM17-bsd nda3KM311*	Lab stock
Figure S6		
709	*h+ ura4-294::prom par1-TAP-par1::ura4 Δpar1::kanMX6*	Lab stock
Figure S7		
148	*h- wt*	Lab stock
1747	*h- rum1BM1AA*	This study
1806	*h- 3HA:ste9*	Modified from Sergio Moreno
1748	*h- 3HA:ste9 rum1BM1AA*	This study

TRANSPARENT METHODS

Cell culture and growth

The strains used in this study are listed in Table S1. All strains were prototrophic and all experiments were performed using early exponential cells grown in Edinburgh minimal medium (EMM) containing NH_4Cl 93.5 mM as the source of nitrogen without supplemented amino acids (Moreno *et al*, 1991). For nitrogen starvation experiments, cells were collected by filtration and washed with four volumes of Edinburgh minimal medium without NH_4Cl (EMM-N) before resuspending them in EMM-N. Control cells were washed with EMM and resuspended in fresh EMM.

When using temperature sensitive alleles, cells were grown at 25°C before shifting them to the restrictive temperature: the *cdc10-V50* mutant was incubated at 32°C, and the experiments with mutants containing the *wee1-50* allele were incubated at different temperatures, as indicated in the figures.

Mating assays

Mating assays were performed in liquid culture. Early exponential cells grown at 25ºC in EMM were collected by centrifugation and washed with three volumes of EMM-N before resuspending them in EMM-N to a final concentration of 5 x 10^6 cells/ml. These cultures were subsequently incubated at 25°C and samples were collected at the indicated time points. After gentle sonication the number of zygotes (Z) and tetrads (T) per 300 non-mating cells (C) were counted and mating efficiency was calculated using the following formula:

$$\frac{(Z+T)\times 2}{(Z+T)\times 2+300}\times 100$$

Flow cytometry

About 10^7 cells were collected by filtration, fixed in 70% ethanol, processed for flow cytometry according to published nuclei isolation protocols (Willis & Rhind, 2011) and stained with propidium iodide (16 µg/ml). Data was collected using a BD FACSCanto™ II instrument, and analyzed using FlowJo (https://www.flowjo.com/).

Cell imaging

For cell wall and DNA staining, about 10^7 of cells fixed in 70 % ethanol were washed with Phosphate-buffered saline (PBS) and resuspended in 1.5 µl of 5 mg/ml calcofluor (Bayer), 2 µl of 1 mg/ml DAPI (4′,6-diamidino-2-phenylindole) and 2 µl of PBS. Cell imaging was carried out using a Cell Observer High Speed fluorescence microscope (Zeiss) equipped with a Hamamatsu ORCA-Flash 4.0 camera and a Plan/Apo 100x (N.A 1.46) oil objective. Images were acquired with the Zen (https://www.zeiss.com/) software and processed using Zen, Fiji (http://fiji.sc/) and Adobe Photoshop CS6 (Adobe Systems, San Jose, CA) softwares.

Genetic manipulation, strain construction and plasmids

Gene deletion, promoter exchange and gene tagging were carried out using PCR cassettes amplified from pFA6a derivative plasmids.

Double mutants were constructed by genetic cross and tetrad dissection.

For the construction of the *nmt41-3PK-miniAID-par1* strain, the auxin inducible degron background strain (*Padh15-skp1-At-Tir1-2NLS Padh15-sk1-Os-Tir1*) was transformed with a PCR cassette amplified from the plasmid pFA6a-*KanMX6-p41nmt1-3PK-miniAID* (Kubota *et al*, 2013; Martín *et al*, 2017) using primers containing 80 bp regions of homology to the sequence directly upstream of the *par1* start codon and to the N-terminal codons of *par1*.

For the construction of the *rum1 BM1AA* strain, *rum1* gene was first deleted using an *ura4*$^+$ cassette, in an *ura4-D18* background. The whole genomic sequence spanning from 300 bp upstream of the start codon to 300 bp downstream of the stop codon was synthesized by GenScript and cloned in a pUC19 backbone. The plasmid was modified using QuikChange II Site-directed mutagenesis kit from Agilent for the generation of the mutated sequence containing I42 to A and E44 to A modifications. Digestion of the plasmid with SalI/SacI released a 1293 bp fragment containing the genomic sequence of *rum1 BM1AA* flanked by the regions upstream of the start codon and downstream of the stop codon. This fragment was then used to transform the *rum1*Δ::*ura4* strain, and clones that had exchanged the *ura4*$^+$ cassette for the mutated allele of *rum1* were selected based on their ability to grow on 5-

fluoroorotic acid (FOA) plates supplemented with uracil. The presence of the I42A and E44A mutations was confirmed by sequencing.

For the construction of the strains expressing the Par1-inhibitor and mock-inhibitor, the *GFP-B56-SliM* sequence (Fig. S5A) was synthetized by GenScript and cloned in a pUC19 vector. Digestion of the plasmid with NdeI/BamHI released a 783 bp fragment containing the *GFP-B56-SLiM* sequence. This sequence was cloned in a pREP1 plasmid and modified to produce the *GFP-B56-SLiM-AA* sequence using QuikChange II Site-directed mutagenesis kit from Agilent. The obtained plasmids were transformed into a *leu1-32* strain and the presence of the adequate sequences was confirmed by sequencing.

The NTAP-Par1 strain was obtained by transformation of *Δpar1::kanMX6 ura4-294* with pJK210-*par1_Prom-NTAP-par1-par1_3'UTR* that had been digested with Stu1 for integration at the *ura4* locus. To obtain the plasmid, the different fragments corresponding to the promoter region and 5'UTR (starting 944 bp upstream of the start codon and finishing at the start codon), the NTAP tag (including a 9 Gly linker) and the genomic sequence with 3'UTR of *par1* (starting at the start codon and finishing 231 bp downstream of the stop codon) were obtained by PCR. Genomic DNA was used as template to amplify the promoter and the genomic sequence followed by 3'UTR of *par1*. For the amplification of the NTAP we used a pcDNA3-NTAP plasmid as template. Each PCR reaction was carried out with primers that introduced 15 bp of homology to the adjacent region of the final plasmid. These three PCR reactions were cloned by recombination using a recombination-mediated cloning kit (In-Fusion® Cloning Kit, Takara-Clontech) in a pJK210 empty vector that had been linearized by PCR.

For the construction of the NTAP-Par1F314Q strain the *par1Δ::KanMX6 ura4-294 leu1-32* strain was transformed with the plasmid pJK210-*par1_Prom-NTAP-par1F314Q-par1_3'UTR* that had been digested with Stu1 for integration at the *ura4* locus. The pJK210-*par1_Prom-NTAP-par1-par1_3'UTR* plasmid was modified to produce the *par1F314Q* sequence using QuikChange II Site-directed mutagenesis kit from Agilent. The presence of the desired sequence in the strain was confirmed by sequencing.

Drugs

A 500 mM stock solution of 1-Naphthaleneacetic acid potassium salt (ChemCruz Biochemicals, SC-229803) was prepared in water and added to a final concentration of 1 mM.

Protein extraction and western blotting

Samples were collected by filtration and washed in STOP buffer (150 mM NaCl, 50 mM NaF, 10 mM EDTA, 1 mM sodium azide) before freezing them in liquid nitrogen. Protein extracts were prepared using the TCA method (Foiani *et al*, 1994). 30 µg of total protein was loaded on Criterion™ TGX™ Any kD™, 7.5 %, 10 % or 12 % gels (Bio-Rad) and transferred to PVDF membranes using a semi-dry blotting system (Trans-Blot® Turbo™ from Bio-Rad). Antibody solutions were prepared in TBS-Tween (0.1 %) containing 5 % BSA (for the anti phospho-p44/p42) or 5 % non-fat milk (for all other antibodies). Western blots were developed using Amersham and Bio-Rad ECL western blotting detection reagents.

Protein purification

E. coli BL21 cells were transformed with a modified version of the pST50Trc1-HISNDHFR plasmid lacking the 6His tag and the TEV site and containing the full length *rum1* gene. Positive colonies were selected on Lysogeny broth (LB) plates supplemented with 100 µg/ml of ampicillin. 10 L of bacterial culture was grown in 2XYT medium, supplemented with 100 µl/ml ampicillin, at 37 °C until OD_{600} reached values between 0.6–0.8. Protein expression was induced by adding 0.5 mM of isopropyl β-D-1-thiogalactopyranoside (IPTG) to the cell culture, and the culture was incubated at 37 °C for 3 hours. Harvested cells were lysed in a buffer containing 50 mM Tris pH 7.5, 50 mM NaCl and protease cocktail inhibitors. The lysate was cleared by centrifugation and passed through a Hi-trap Q anion exchanger column, 5 ml bed volume. Rum1 was collected in the flow through, which was then dialyzed against a buffer containing 20 mM Hepes pH 7.5 and 50 mM NaCl. The dialyzed protein sample was loaded in a cation exchanger Mono S column, 5 ml bed volume, and eluted with a linear salt gradient from 50 mM to 500 mM of NaCl. The eluted fractions of Rum1 were pooled together, concentrated and injected in a Hi-Load Superdex S200

16/600, previously equilibrated with 50 mM Tris pH 7.5 and 100 mM NaCl. Purified Rum1 was concentrated to 5 mg/ml, glycerol was added to reach 50 % v/v final concentration and the protein was stored at -80 °C until further use.

E. coli BL21 cells were transformed with a pST50Trc1-HISNDHFR plasmid containing the full length *Ste9*, to generate 6His-Ste9. 15 L of bacterial culture was grown in 2XYT media, supplemented with 100 µl/ml ampicillin, at 37 °C until OD_{600} reached values between 0.6–0.8. At that time, protein expression was induced with 0.75 mM IPTG and the culture was incubated at 37 °C for 3 hours. Harvested cells were lysed in a buffer containing 20 mM phosphate buffer pH 8, 300 mM NaCl and protease cocktail inhibitors. The lysate was cleared by centrifugation and loaded in a 5 ml Nickel column, followed by column wash with the same buffer used for cell lysis. The bound protein was eluted with a linear gradient from 0 to 500 mM of imidazole. The fractions containing Ste9 were dialyzed against a buffer containing 20 mM phosphate buffer pH 7.5 and 50 mM NaCl. The dialyzed protein sample was loaded in a cation exchanger Mono S column, 5 ml bed volume, and eluted with a linear salt gradient from 50 mM to 500 mM of NaCl. The eluted fractions of Ste9 were pooled together and dialyzed against a buffer containing 20 mM phosphate buffer pH 7.5 and 50 mM NaCl. The dialyzed protein was concentrated, mixed with glycerol to reach 50 % v/v and stored at -80 °C.

Immunopurifications

300 ml of exponentially growing cells (~10^9 cells) were collected by filtration, and pellets were washed in STOP buffer before freezing them in liquid nitrogen. Native protein extraction was performed in immunopurification (IP) Buffer (20 mM Tris-HCl pH 8, 140 mM KCl, 1.8 mM $MgCl_2$, 0.1 % NP40, 1 mM PMSF, 2 cOmplete™ mini protease inhibitors tablets (Roche)/10 ml buffer, 1 phosSTOP™ tablet (Roche)/10 ml buffer).

Cells were broken using a FastPrep®-24 equipped with a CryoPrep™ adapter for cryogenic lysis. For the TAP purifications, 10 mg of whole cell extract was incubated at 4 ºC for 1 h with 75 µl of Dynabeds® Pan Mouse IgG (Invitrogen) which had been incubated overnight with anti-protein A antibody in a 1:250 dilution. For the purification of proteins tagged with GFP, 50 µl of GFP-Trap Magnetic Agarose beads (ChromoTek) were incubated between 15 and 60

minutes with 10 mg of whole cell extracts. The beads were then washed 4 times with Wash Buffer (20 mM Tris-HCl pH 8, 140 mM KCl, 1.8 mM $MgCl_2$, 0.04 % NP40, 10 % glycerol) containing 1 mM PMSF and 4 times with Wash Buffer containing 1 mM DTT. The beads were finally resuspended in Laemmli loading buffer (for co-inmunopurification experiments).

To assay the ability of Rum1 and Ste9 homogenous recombinant purified proteins to bind to TAP-Par1, TAP-Par1 attached to the beads was washed once with Wash Buffer containing high concentration of salt (20 mM Tris-HCl pH 8, 500 mM NaCl, 1.8 mM $MgCl_2$, 0.04 % NP40, 10 % glycerol). After that, the beads were washed with standard Wash Buffer 3 times to remove the salt and incubated for with 50–100 ng of purified protein at 4 ºC for 1 hour. The beads were washed 5 times with Wash Buffer containing 1 mM DTT. Afterwards, the beads were resuspended in Wash buffer containing 1 mM DTT and 20 U AcTEV (Invitrogen) and incubated at room temperature for 1 h to release the CBP-tagged protein from the protein A.

7 mg of Rum1 recombinant protein were coupled to Amine-Terminated Peptide Conjugation Magnetic Beads (LifeTein) following the protocol of the supplier. 10 mg of whole cell extract was incubated with 75 µl of the Rum1-beads at 4 ºC for 1 h. The beads were then washed 3 times with Wash Buffer (20 mM Tris-HCl pH 8, 140 mM KCl, 1.8 mM $MgCl_2$, 0.04 % NP40, 10 % glycerol) containing 1 mM PMSF and 4 times with Wash Buffer containing 1 mM DTT and 0.1 % of Tween20. The beads were finally resuspended in Laemmli loading buffer.

Antibodies

Polyclonal anti Gad8S546-P antibody was produced in rabbit by Eurogentec and used in a 1:500 dilution for western blotting. The Rum1 antibody was purified from the serum (R4) (a kind gift from Jacky Hayles) using Rum1-coupled magnetic beads and used in a 1:1000 dilution for western blot. The Ste9 serum (SM4) (a kind gift from Sergio Moreno) was used in a 1:1000 dilution in western blot to detect purified Ste9. The following commercial antibodies were used for western blotting: anti-Cdc13 (Abcam) 1:1000, anti-Cig2 (Abcam) 1:1000, anti-phospho-Cdc2 (Cell Signaling), anti-β-actin (Abcam) 1:1000, anti α-tubulin (SIGMA) 1:30000, anti-PSTAIR (Abcam) 1:1000, anti-phospho S/T AKT substrate (PAS) (Cell Signaling) 1:1000, anti-V5

(AbD Serotec) 1:1000; anti-GFP (Abcam) 1:1000, anti-phospho-S6K (T389) mouse monoclonal antibody (clone #1A5) (Cell Signaling) 1:1000 was used to detect phosphorylated Psk1; anti phospho-p44/p42 (Cell Signaling) 1:1000 was used to detect phosphorylated Spk1; anti-CBP (GenScript) 1:1000; anti-HA 12CA5 (Biolegends) 1:500; HRP-conjugated anti mouse IgG (SIGMA) 1:10000 and HRP-conjugated anti rabbit IgG (SIGMA) 1:10000. To avoid IgG detection in IP experiments, Rabbit and Mouse Trueblot® (Rockland) secondary antibodies were used.

RNA extraction and quantitative PCR (qPCR)

For qPCR experiments, 20 ml samples were collected by centrifugation and pellets were washed in DEPC-treated water before freezing them in liquid nitrogen.

Total RNA preparation was performed with MasterPure™ Yeast RNA Purification Kit (Epicentre) following the manufacturer's instructions. For qPCR experiments, 1 µg of RNA was used for cDNA synthesis using SuperScript® III Reverse Transcriptase (Invitrogen). qPCR was performed with the corresponding oligoes, *mei2*: AAGAAACTCCCACTGCTGCT and CTGGAGATGATTCAGTGCGT, *rum1*: CCCAAACTCTTGTTTGCTGA and AGGGAGAATGCCAATTTGAG and *act1*: CAAATCCAACCGTGAGAAGA and CATCACCAGAGTCCAAGACG with SYBR® Select Master Mix (Applied Biosystems). Analysis was done using the ΔΔCt method.

Supplemental references

Foiani M, Marini F, Gamba D, Lucchini G & Plevani P (1994) The B subunit of the DNA polymerase alpha-primase complex in Saccharomyces cerevisiae executes an essential function at the initial stage of DNA replication. *Molecular and cellular biology* **14:** 923–933

Kubota T, Nishimura K, Kanemaki MT & Donaldson AD (2013) The Elg1 replication factor C-like complex functions in PCNA unloading during DNA replication. *Molecular cell* **50:** 273–280

Martín R, Portantier M, Chica N, Nyquist-Andersen M, Mata J & Lopez-Aviles S (2017) A PP2A-B55-Mediated Crosstalk between TORC1 and TORC2 Regulates the Differentiation Response in Fission Yeast. *Current biology : CB* **27:** 175–188

Moreno S, Klar A & Nurse P (1991) Molecular genetic analysis of fission yeast Schizosaccharomyces pombe. *Methods in enzymology* **194:** 795–823

Willis N & Rhind N (2011) Studying S-phase DNA damage checkpoints using the fission yeast Schizosaccharomyces pombe. *Methods Mol Biol* **782:** 13–21